Oceanologia, corrected, in press
Polish Academy of Sciences
Institute of Oceanology
Open access article under the CC BY license
https://doi.org/10.5697/FIXM1200

Chlorophyll *a* distribution in the Arabian Gulf: climate, trends, and global teleconnections

Cheriyeri Poyil Abdulla[1], Valliyil Mohammed Aboobacker[1,*], Muhammad Shafeeque[2], Ponnumony Vethamony[1]

Abstract
The study examined the climatology, trends, and variability of chlorophyll *a* (hereafter referred to as 'Chl *a*') concentration in the Arabian Gulf (hereafter referred to as 'Gulf'), utilizing merged satellite datasets for the period 1998–2022. Distinct spatial and temporal variabilities were identified, which are linked to climatic features, inflow from the Arabian Sea, freshwater discharge into the Gulf, and the Gulf circulation. The study identified an opposing phase in the dominance of Chl *a* between the southern Iranian coast and the Arabian coast. Among wind speed, sea level anomaly, and sea surface temperature (SST), multiple linear regression analysis revealed SST as the strongest predictor of phytoplankton growth. The La Niña and positive Indian Ocean dipole (IOD) phases enhanced the Chl *a*, while El Niño and negative IOD phases caused its decline. The Chl *a* increased in the northern coast and southern shelf of the Gulf, of the order of 0.017–0.031 mg/m^3/y, while the southern Iranian coast exhibited weaker negative trends.

Keywords
Arabian Gulf; GlobColour; Chlorophyll *a*; Primary productivity; Gulf circulation; Climatic indices

[1]*Environmental Science Center, Qatar University, P.O. Box. 2713, Doha, Qatar*
[2]*Applied Research Center for Environment and Marine Studies, King Fahd University of Petroleum & Minerals, Dhahran 31261, Saudi Arabia*
[*]**Correspondence**: vmaboobacker@qu.edu.qa (V. M. Aboobacker)

Received: 20 March 2025; **revised:** 9 November 2025; **accepted**: 17 November 2025

1. Introduction

Chlorophyll *a* (Chl *a*) serves as a vital pigment in photosynthetic organisms, reflecting their abundance and primary productivity levels in aquatic environments (Behrenfeld and Falkowski, 1997). Remote sensing-based Chl *a* concentration data play a crucial role in monitoring and understanding marine ecosystems (Shafeeque et al., 2021a). These observations provide valuable insights into phytoplankton dynamics, primary productivity, and ecosystem health, which benefit studying climate change impacts, assessing oceanic biogeochemical processes, identifying phytoplankton blooms, detecting harmful algal events, and measuring the impact of environmental stressors on marine environments (Al-Naimi et al., 2017). Satellite remote sensing methods have provided unprecedented global insights into Chl *a* spatial and temporal distribution (Vantrepotte and Mélin, 2009; Westberry et al., 2023; Xi et al., 2020). Studies have elucidated the role of climatic phenomena, including El Niño and La Niña events, in driving significant global variations in Chl *a*, affecting phytoplankton productivity patterns across different oceanic regions (Currie et al., 2013; Shafeeque et al., 2021b). Additionally, research has indicated that global warming trends could be altering ocean stratification, potentially leading to decreased nutrient upwelling and thus influencing global Chl *a* (Gao et al., 2018).

The Arabian Gulf (hereafter 'Gulf') is one of the most biologically and geologically distinct marine environments in the world (Price et al., 1993; Ross et al., 1986; Sheppard et al., 2010). Geographically, the Gulf is bordered by Saudi Arabia, Kuwait, Iraq, Iran, Qatar, the United Arab Emirates, and Oman. The Gulf is an important body of water for international trade and energy resources and has geopolitical significance in the region. Its uniqueness, including semi-enclosed nature, extreme salinity levels, high-temperature variations, and limited freshwater input, makes it an important region for studying marine processes under extreme conditions. The Gulf's waters support diverse and economically important marine ecosystems, including coral reefs, seagrass beds, and fisheries, which are under increasing stress due to anthropogenic activities and climate change (Keshavarzifard et al., 2021; Vaughan et al., 2019). The Gulf experiences extreme conditions with a hot and arid climate, excess evaporation over precipitation, elevated temperatures, and high salinity levels (Aboobacker et al., 2024a; Al-Ansari et al., 2022; Elobaid et al., 2022; Rakib et al., 2021; Reynolds, 1993), which significantly influence phytoplankton community structure and productivity (Al-Said et al., 2017; Polikarpov et al., 2016; Rao and Al-Yamani, 1998). The estimated residence time of the Gulf water is 3–5 years with an inflow of 2696 km^3/y and an outflow of 2375 km^3/y (Reynolds, 1993). The circulation is mainly driven by winds, density gradients, and the water exchange with the Indian Ocean that occurs through the Strait of Hormuz (Kämpf and Sadrinasab, 2006; Mussa et al., 2024; Thoppil and Hogan, 2010). The major components of surface circulations are the northwestward-flowing Iranian Coastal Current (ICC) and the southeastward-flowing Arabian Coastal Current (ACC), while the density-driven deep currents flow towards the southeast from the northern Gulf to the Sea of Oman through the Strait of Hormuz.

The variability of Chl *a* in the Gulf is characterized by unique hydrographic, geomorphological, and ecological conditions. In addition, anthropogenic effects may result in high levels of Chl *a* and lead to eutrophication in Gulf coasts (Al-Yamani et al., 2020; Devlin et al., 2019). In Kuwait waters, Chl *a* was analyzed using in situ observations and discussed the local seasonal variations and the impact of anthropogenic activities (Al-Yamani et al., 2020). Al-Thani et al. (2023) evaluated the physical parameters that control the Chl *a* distribution in the Exclusive Economic Zone (EEZ) of Qatar and analyzed the spatio-temporal variability using in situ measurements from various transects. Nezlin et al. (2010) utilized SeaWiFS data (1996–2009) and reported that Chl *a* levels in the Gulf are significantly influenced by local meteorological and oceanographic factors, including vertical stratification, precipitation, and aeolian dust transport. Similarly, Moradi (2020) and Bordbar et al. (2024) utilized MODIS data and reported that sea surface temperature (SST) and winds influence Chl *a* variability in the Gulf. Given the Gulf's strategic importance as a global oil hub and its proximity to densely populated coastal regions, a detailed understanding of the patterns and drivers of Chl *a* distribution is essential for predicting and mitigating the impacts of human activities on marine ecosystems. Our research leveraged the longest available satellite dataset of Chl *a* for the Gulf to conduct a detailed investigation of the spatiotemporal distribution of Chl *a* in the Gulf. The study also discussed the relationships between observed Chl *a* distribution and global climate oscillations. This study enhances the temporal resolution and spatial coverage of the analysis, providing a more comprehensive understanding of Chl *a* dynamics over an extended period.

To quantify the impact of various environmental parameters on Chl *a*, this study employs multiple linear regression analysis, a sophisticated statistical technique that allows for the examination of the relationship between multiple independent variables and the dependent variable (Chl *a*). To understand the potential influence of global climatic oscillations on the observed Chl *a* pattern, we have investigated the impact of El Niño-Southern Oscillation (ENSO), Indian Ocean Dipole (IOD), and North Atlantic Oscillation (NAO). These events are known for impacting many of the marine ecosystems of the World Ocean (Currie et al., 2013; Racault et al., 2017; Shafeeque et al., 2021b) and have influenced the Gulf ecosystem by altering SST, wind patterns, nutrient upwelling, etc., which in turn influence Chl *a* (Aboobacker et al., 2021b; Al Senafi, 2022; Al-Subhi and Abdulla, 2021; Niranjan Kumar and Ouarda, 2014). The sections in this paper are arranged as follows: Section 2 describes the study area and its features; the material and methods are described in Section 3, results are discussed in Section 4, and the findings are summarized in the final section.

2. Study area

The Gulf, situated between 47.5°E–56.5°E and 23.5°N–30.5°N, encompasses an area of approximately 241,000 km^2. This semi-enclosed marginal sea of the Indian Ocean stretches about 1,000 km in length, with its width varying from 56 km at its narrowest point in the Strait of Hormuz to 338 km at its widest. The Gulf is characterized by its shallow nature, with an average depth of 36 m, although it reaches a maximum depth of 110 m in the Strait of Hormuz. The Gulf's bathymetry features a southward widening channel that extends from the Strait of Hormuz across a series of sills and shallow basins to the shelf edge (Elobaid et al., 2022; Kämpf and Sadrinasab, 2006). Tectonic-driven subsidence has resulted in a deeper seafloor on the southern part of the Strait, forming a 70–95 m deep trough along the Iranian coast in the eastern part of the Gulf. This asymmetry is further emphasized by the presence of a shallow bank area (depth < 20 m) in the southwestern Gulf, contrasting with a deeper area in the Iranian waters. The narrow Strait of Hormuz plays a crucial role in restricting water exchange between the Gulf and the northern Indian Ocean.

The region experiences distinctive wind patterns, with the northwesterly Shamal being the dominant wind system. Other significant wind types include the northeasterly/easterly Nashi winds and the southeasterly/southerly Kaus winds (Aboobacker et al., 2021a). The Gulf's surface circulation is dominated by ICC and ACC, with the ICC exhibiting relatively stronger flows compared to the ACC. Seasonal variations in current speeds are evident, with summer currents generally stronger than winter currents. The Gulf experiences its strongest currents during May and June. Additionally, prominent eddies are observed in both winter and summer seasons, contributing to the complex circulation patterns within the Gulf (Mussa et al., 2024).

The primary freshwater input comes from the Shatt-Al-Arab river system in the north, fed by the Euphrates, Tigris, and Karun rivers. Historically, the annual mean discharge of the Shatt-Al-Arab was between 35 km^3/y (Johns et al., 2003; Saad, 1978) to 45 km^3/y (Wright, 1974). However, this discharge has been substantially reduced over the years due to extensive dam construction upstream. More recent measurements indicate a discharge of 40–70 m^3/s (Alosairi and Pokavanich, 2017), which is equivalent to approximately 1.26–2.21 km^3/y. A key hydrological characteristic of the Gulf is its high evaporation rate, estimated at approximately 2 m/y per unit surface area (Ahmad and Sultan, 1991; Privett, 1959), which significantly exceeds both precipitation and river discharge (Johns et al., 2003). The Gulf's unique hydrodynamics are characterized by a reverse estuarine circulation, primarily driven by excessive evaporation. This circulation pattern results in a dense bottom outflow that follows the southern coastline, while an inflow of Indian Ocean Surface Water (IOSW) moves along the Iranian coastline (Johns et al., 2003; Reynolds, 1993). The geographical location of the study area is shown in Figure 1. For a detailed analysis of variability in the Gulf, we have selected five locations as shown in Figure 1. The selected locations (P1–P5) were chosen to be representative of the major coastal regions and Chl *a* dynamics within the Gulf. P1 represents the northern Gulf and the region of Shatt Al-Arab river discharge; P2 and P3 represent the Arabian coast of the Gulf; P4 and P5 represent the Iranian coast of the Gulf. By including these locations, we aimed to capture the major spatial patterns and drivers of Chl *a* variability across the Gulf. As indicated, the selection was based on examining the climatology of annual mean and seasonal mean Chl *a*, the variations are assessed and based on these results, the stations are selected for detailed discussion, in such a way that the stations cover the general features of Iranian and Arabian coasts.

3. Data and methods

3.1 Data

3.1.1 Chlorophyll *a*

This study utilizes the GlobColour Chl *a* concentrations obtained from the Copernicus Marine Environment Monitoring Service (CMEMS) database, with the product ID: https://data.marine.copernicus.eu/product/OCEANCOLOUR_GLO_BGC_L4_MY_009_104/services (last accessed on 1 December 2024; https://data.marine.copernicus.eu/product/OCEANCOLOUR_GLO_BGC_L4_MY_009_104/services; DOI: https://doi.org/10.48670/moi-00281). This is a composite product derived from the integration of multiple satellite sensors, including SeaWiFS, MODIS, MERIS, VIIRS-SNPP&JPSS1, and OLCI-S3A&S3B (Veny et al., 2024). By merging data from these various sensors, the product ensures a high level of accuracy and consistency in the Chl *a* measurement. The dataset features a fine spatial resolution of 0.04° × 0.04°, which allows for detailed mapping of Chl *a* in the Gulf. Moreover, the dataset was updated daily, providing a temporal resolution that supports continuous monitoring and analysis of oceanographic conditions. For this study, monthly Chl *a* concentrations were extracted for the period 1998–2022.

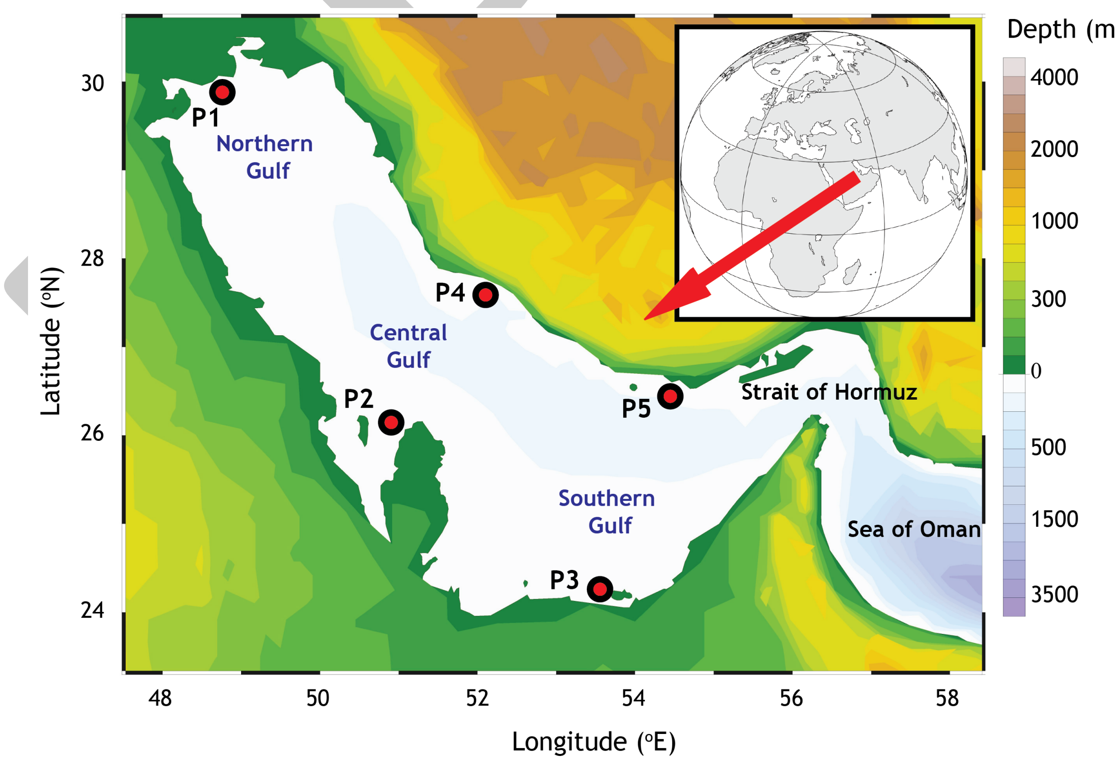

Figure 1. Study area. The selected stations for time series analysis are marked with red dots.

3.1.2 Wind

ERA5, the fifth generation of global climate and weather reanalysis produced by the European Centre for Medium-Range Weather Forecasts (ECMWF), offers a comprehensive dataset that spans from 1940 to the present, providing extensive temporal coverage for climate and weather research (Hersbach et al., 2020). ERA5 winds are available at a horizontal resolution of 0.25° × 0.25° and for temporal resolutions of hourly, daily, and monthly, offering detailed spatial and temporal insights into wind patterns. In this study, we downloaded the monthly winds in the Gulf for the period 1998–2022 (https://cds.climate.copernicus.eu/datasets/reanalysis-era5-single-levels-monthly-means?tab=overview; last accessed on 1 December 2024). This data has been used to delineate its role on the Chl *a* distribution in the Gulf. Earlier, ERA5 winds along the coast of Qatar were verified and utilized for the wind energy resource assessment (Aboobacker et al., 2021b). Additionally, ERA5 winds were validated in the Gulf against the observations from the oceanographic buoys (Mahmoodi et al., 2019).

3.1.3 Sea Surface Temperature

SST datasets employed in this study were derived from the Advanced Very High-Resolution Radiometer (AVHRR) Pathfinder Version 5, available from NASA's Physical Oceanography Distributed Active Archive Center (PO.DAAC). AVHRR, a space-borne sensor, has been instrumental in measuring SST by detecting thermal infrared radiation emitted by the ocean surface. This technique allows for accurate and reliable temperature measurements, essential for understanding various oceanographic and climatic processes (https://podaac.jpl.nasa.gov/dataset/, last accessed on 1 December 2024; Saha et al., 2018). The Pathfinder SST provides daily daytime observations at a high horizontal resolution of 0.04° × 0.04°, enabling detailed spatial analysis of sea surface temperature variations across the globe. The AVHRR Pathfinder SST dataset offers continuous temporal coverage, which is crucial for monitoring both short-term and long-term changes in SST. This dataset is particularly valuable for its consistency and accuracy, achieved through rigorous calibration and validation processes. The AVHRR SST data are available from 1981 to the present, from daily to monthly time scales. In this study, we used the monthly AVHRR SST during 1998–2022 to analyze how SST variations within the Gulf affect the Chl *a* change.

3.1.4 Sea Level Anomaly

Sea Level Anomaly (SLA) datasets utilized in this study were sourced from AVISO (Archiving, Validation, and Interpretation of Satellite Oceanographic data) through the Copernicus Marine Environment Monitoring Services (CMEMS). The product (ID: SEALEVEL_GLO_PHY_L4_MY_008_047) provides high-quality SLAs derived from multiple altimeter missions, including TOPEX/Poseidon, Jason-1, Jason-2, Jason-3, Envisat, ERS-1, ERS-2, and SARAL/AltiKa, among others (https://data.marine.copernicus.eu/product/SEALEVEL_GLO_PHY_L4_MY_008_047/services; Chinta et al., 2024). It is crucial for understanding sea level variations and their implications. The data is for a horizontal resolution of 0.25° × 0.25° and a temporal resolution of daily and monthly from 1993 to the present. We used monthly SLA during 1998–2022 to understand the role of SLA on Chl *a* within the Gulf (last accessed on 1 December 2024).

3.2 Methods

3.2.1 Multiple linear regression

Multiple linear regression analysis was carried out with Chl *a* as the dependent variable, and SST, SLA, and wind speed as independent variables. We used box-averaged data for all the selected point locations. This analysis evaluates how multiple independent variables influence a dependent variable simultaneously. It quantifies the individual impact of each independent variable on the dependent variable while controlling for the effects of other variables included in the model, as represented in Equation (1).

$$y_i = \beta_0 + \beta_1 x_{i1} + \beta_2 x_{i2} + \ldots + \beta k_{xi} k + \epsilon_i, \quad i = 1, 2, \ldots, n \quad (1)$$

where β_0, β_1, β_2 represents the random error, allowing each response to deviate from the average value of y. These errors are presumed to be independent, with a mean of zero and a common variance (σ^2) and follow a normal distribution.

3.2.2 Long-term linear trend

The trend analysis and significance test of the observed trends were conducted using Sen's slope estimator (Sen, 1968) and the Mann-Kendall test (Kendall, 1975), respectively. These statistical methods are robust and widely used in environmental and climatic studies to identify and quantify trends in time series data. Sen's slope estimator is a non-parametric method used to determine the magnitude of a trend. Sen's slope is calculated as the median of the slopes of all possible pairs of data points, providing a reliable estimate of the true slope of the trend (Sen, 1968). The Mann-Kendall test is a non-parametric test used to assess the significance of a trend in a time series. This test evaluates the null hypothesis that there is no trend against the alternative hypothesis that a trend exists. It is based on the ranks of the data rather than the actual values, making it robust against non-normal distributions and missing values (Kendall, 1975).

3.2.3 Composite analysis

To examine the typical Chl *a* response to specific climate events, we performed a composite analysis. For each climate index (ENSO, IOD, and NAO), we first identified years corresponding to specific phases (e.g., El Niño, La Niña, positive IOD, negative IOD, positive NAO, and negative NAO). Then, for each event phase, we extracted the annual mean

Table 1. Coordinates of the sampling stations.

Station	Latitude	Longitude
S0	25.299°N	51.521°E
S1	25.310°N	51.542°E
S2	25.350°N	51.554°E
S3	25.320°N	51.583°E
S4	25.322°N	51.627°E
S5	25.283°N	51.646°E
S6	25.321°N	51.676°E
S7	25.294°N	51.708°E
S8	25.408°N	51.645°E
S9	25.383°N	51.570°E
S10	25.435°N	51.563°E

Chl *a* values for the Gulf during those years and calculated the composite mean. This involved averaging the annual mean Chl *a* values across all years identified for that specific event phase. By aggregating data from multiple years of the same event, the composite analysis aims to reduce the influence of interannual variability and highlight the characteristic spatial and temporal patterns in Chl *a* associated with each climate mode, which might be unnoticed while analyzing individual years.

For the data analysis and visualization presented in this paper, the following software and tools were employed: FERRET (Hankin et al., 1996), CDO (Schulzweida, 2023), R (R Core Team, 2023), and MATLAB (The MathWorks Inc., 2024).

4. Results and discussion

4.1 Verification of GlobColour Chl *a*

The GlobColour project employs a comprehensive validation approach, comparing merged sensor products with in situ measurements to assess their accuracy and consistency (Garnesson et al., 2025). The global 4 km GlobColour product demonstrates a good relationship between satellite-derived Chl *a* and in situ measurements, with a coefficient of determination (R^2) of 0.75 for daily data. The cloud-free (interpolated) product shows a slight degradation but still achieves an R^2 of 0.71 (Garnesson et al., 2025, see Table 3). These statistics, based on many available in situ measurements, demonstrate the quality of the GlobColour product for a wide range of applications (Garnesson et al., 2025). The utility of GlobColour data for studying Chl *a* and primary productivity is well-established, with applications spanning diverse ocean basins and including studies of the adjacent Mediterranean Sea, demonstrating its relevance to the Gulf (El Hourany et al., 2019; Ford and Barciela, 2017; Ford et al., 2012; Maritorena et al., 2010; Pramlall et al., 2023; Pitarch et al., 2016; Yu et al., 2023).

The accuracy of GlobColour Chl *a* data within the Qatar waters has been verified against available in situ data collected using CTD at 11 stations, encompassing both coastal and offshore areas of Doha (as detailed in Table 1). Data from December 2021, June 2022, and March 2023, were used for comparison. The findings, summarized in Table 2 indicate that GlobColour Chl *a* values align reasonably well with in situ measurements, although there is a slight overestimation at lower concentrations. For instance, in December, the mean (maximum) Chl *a* recorded by GlobColour was 1.18 mg/m^3 (1.65 mg/m^3), while in situ measurements were slightly lower at 1.15 mg/m^3 (1.88 mg/m^3). Nonetheless, the limitations in the availability of in situ data in the Gulf lack a comprehensive overview of the validation of CMEMS Chl *a* data. However, this data has been validated against in situ measurements in other areas quite satisfactorily (Amorim et al., 2024; Garnesson et al., 2019; Moradi, 2021; Volpe et al., 2019).

Several studies have successfully utilized satellite datasets to analyze Chl *a* variability in the Gulf. For instance, Nezlin et al. (2010) employed MODIS and SeaWiFS datasets, demonstrating their usefulness in assessing regional Chl *a* patterns. Moradi and Kabiri (2015) further explored MODIS data, corroborating its effectiveness in capturing Chl *a* dynamics. Alosairi et al. (2019) expanded on these findings by incorporating both MODIS and VIIRS data, providing a comprehensive view of Chl *a* variability. Similarly, the utilization of MODIS data has been noted by other researchers, also highlighting its widespread acceptance and effectiveness in monitoring Gulf waters (Hussein et al., 2021; Moradi and Moradi, 2020). These studies confirm the reliability of satellite-derived Chl *a* data, supporting its application in understanding and managing marine ecosystems in the Gulf despite the limited in situ measurements available for direct validation.

4.2 Annual mean Chl *a* features

Analysis of annual mean Chl *a* in the Gulf reveals notable spatial variations. The annual mean Chl *a* along the northern Iranian coast is relatively lower than that along the Arabian coast (Figure 2). In the nearshore of the northern Iranian coast, the Chl *a* is 1 to 1.5 mg/m^3, suggesting lesser nutrient input from the surrounding areas or different hydrodynamic conditions that affect nutrient distribution and phytoplankton activity. The spatial average of annual mean Chl *a* over the Gulf is 1.1 mg/m^3. About 56% of the Gulf, encompassing mostly offshore waters, has an annual mean Chl *a* of less than 1 mg/m^3, whereas 38% of the region has a concentration between 1 to 2 mg/m^3, and 5% between 2 to 3 mg/m^3. A strong nearshore-offshore gradient in Chl *a* is identified along the coastal regions. This pattern is particularly pronounced along the Arabian coast, where the Chl *a* is reduced from 2 mg/m^3 in the nearshore to less than 1 mg/m^3 in the offshore. Such decrements are quite common and are influenced by various factors, including the processes that make nutrients available in the surface layer, which fosters phytoplankton intensity close to the coast (Anjaneyan et al., 2023; Dai et al., 2023;

Table 2. The GlobColour observations of Chl *a* against in situ data.

Date	GlobColour		in situ	
	Range) (mg/m³)	Mean (mg/m³)	Range (mg/m³)	Mean (mg/m³)
7 December 2021	0.96–1.65	1.18	0.17–1.88	1.15
2 June 2022	0.88–2.76	1.55	0.17–3.22	1.11
2 March 2023	0.54–1.74	0.83	0.33–1.56	0.91

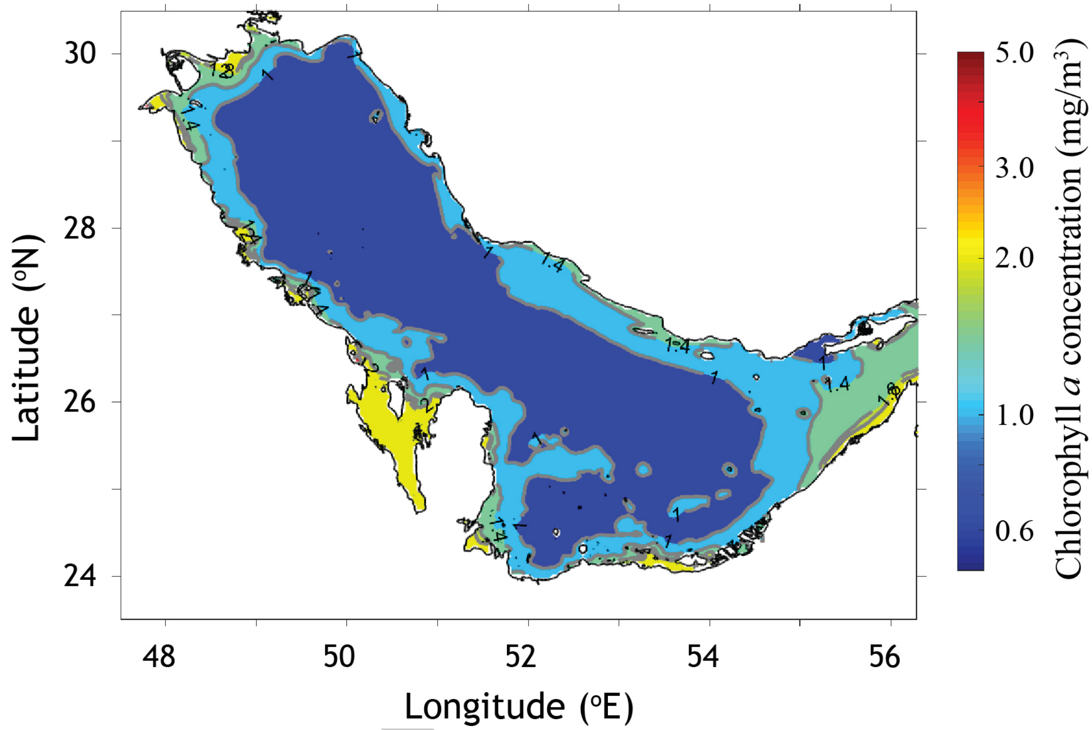

Figure 2. Annual mean Chl *a* for the period 1998–2022.

Kim et al., 2009).

In the north, the higher annual mean Chl *a* concentrations are observed near the Shatt al-Arab river plume (>2.0 mg/m^3). Here, the Euphrates, Tigris, and Karun rivers discharge nutrient-rich waters and promote phytoplankton growth. The Iranian Bay also exhibits high Chl *a* concentration, reflecting favorable conditions for phytoplankton. Notable Chl *a* concentrations are found in Kuwait Bay, of the order of 2.0 mg/m^3 (Devlin et al., 2019; Heil et al., 2001). The Shatt Al-Arab estuarine waters in the north are characterized by high biomass and nutrient-rich conditions, leading to higher productivity but lower species diversity compared to adjacent areas, while Kuwaiti waters demonstrate higher species diversity but lower biomass and production than the Shatt Al-Arab region (Rao and Al-Yamani, 1998). Recent studies have attributed changes in the Gulf's phytoplankton community to nutrient increases (Devlin et al., 2015) and salinity-related fluctuations, particularly in the Northern Gulf region (Al-Said et al., 2017), playing a crucial role in driving the elevated Chl *a* levels and primary productivity observed in the northern Gulf.

The Gulf of Salwa, which shares its coast with Qatar, Bahrain, and Saudi Arabia highlights a remarkable Chl *a* concentration of around 2.0 mg/m^3. The east coast of Qatar exhibits moderate Chl *a* concentrations, in the range of 1.0–1.5 mg/m^3 and higher, which is consistent with the earlier studies (Al-Naimi et al., 2017; Al-Thani et al., 2023; Rajendran et al., 2022). Along the Iranian coast, the Chl *a* is relatively higher in the southern part, adjacent to the Strait of Hormuz. A decrement in Chl *a* patterns is also visible from the Strait of Hormuz towards the central Gulf. This is aligned with the pattern of the nutrient-rich water inflow from the Arabian Sea (Mussa et al., 2024; Ismail and Al Shehhi, 2022). The deeper regions of the Gulf with limited nutrient supply to the euphotic zone exhibit significantly lower Chl *a* concentration, emphasizing the importance of coastal processes in supporting higher productivity in the nearshore waters. However, certain regions along the coast, especially where the discharge of brine is prominent (for instance, the Jubail coast of Saudi Arabia), exhibit lower Chl *a* concentration compared to the adjacent regions. This variability is crucial when shaping the spatial distribution of marine ecosystems since they are subject to anthropogenic stress and resilience.

4.3 Seasonal and monthly mean Chl *a* features

The Gulf exhibits distinct seasonal variations in Chl *a*, demonstrating diverse ecological dynamics influenced by regional climatic conditions and water exchange with the Arabian Sea. The seasons are considered winter (December to March), spring (April to May), summer (June to September), and autumn (October to November). The seasonal variations in Chl *a* concentrations are not uniform across the basin (Figure 3). Winter exhibits higher Chl *a* concentrations in the eastern Gulf, adjacent to the Strait of Hormuz and along the Iranian coast, while a major part of the UAE coast experiences lower Chl *a* concentrations (Figure 3a). Relatively lower Chl *a* is observed in the offshore waters of the northern Gulf, also. The nutrients advected through the Strait of Hormuz are the primary cause for the observed higher Chl *a* in the eastern Gulf, especially along the coastal and offshore waters of central and southern Iran (Moradi and Kabiri, 2015; Nezlin et al., 2010). This extension of nutrient-rich surface waters from the northern Arabian Sea and the Sea of Oman results in notable east-west Chl *a* differences within the Gulf. A similar extension was observed in SST, indicating a relatively warm water inflow to the Gulf during winter (Bordbar et al., 2024). The building up of Chl *a* in the eastern Gulf is also supported by shamal winds, which oppose and limit the northward extension of the ICC (Figure 4a). Therefore, the nutrients get consolidated within the eastern Gulf. The northern head of the Gulf also exhibits higher Chl *a* due to the river discharge from the Shatt-al-Arab River.

As spring sets in, there is a considerable overall decline in Chl *a* across the Gulf, with most of the regions experiencing values below 1 mg/m^3. This period generally marks low values in most of the offshore regions, the Iranian coast, and the UAE coast (Figure 3b). The inflow of Indian Ocean Surface Water (IOSW) is increased compared to winter (Figure 4b). However, the surface layer of the Sea of Oman is in a nutrient-depleted condition during spring (Ershadifar et al., 2023), which results in the significant reduction of Chl *a* within the Gulf. Therefore, the reduction of Chl *a* in the Gulf is primarily attributed to the low nutrient concentrations in the inflow waters. Spring is also characterized by the beginning of stratification in the Gulf, thus the nutrient mixing from the deep layer gets diminished (Alosairi et al., 2011; Reynolds, 1993). However, the northern head of the Gulf and Kuwait Bay have relatively higher concentrations (1–2 mg/m^3) compared to other regions. This is mainly attributed to the nutrient supply from the Shatt-Al-Arab River (Moradi, 2020; Pous et al., 2015). The ACC is stronger during spring (Figure 4b), which enhances the flow of the river-discharged waters along the Arabian coast. The influence of the Shatt-Al-Arab river water in the Gulf is limited to the northwestern Gulf (Al-Mudaffar Fawzi and Mahdi, 2014). Therefore, relatively higher Chl *a* has been observed along the Saudi Arabian coast during this season compared to winter.

The summer and autumn mark the highest mean Chl *a* concentrations (1–2 mg/m^3) along the coast of Kuwait, Saudi Arabia, Bahrain, Qatar, and the UAE (Figure 3c and d). Compared to spring, the offshore waters in the northern and central Gulf also exhibit higher Chl *a* concentrations as the flow of nutrient-rich waters from the Sea of Oman gets intensified. Along the Qatar coast, the highest Chl *a* is observed during summer. This is consistent with earlier studies (Aboobacker et al., 2024b; Elobaid et al., 2022; Rakib et al., 2021). On the other hand, the Chl *a* along the Iranian coast is relatively low during summer and autumn compared to winter. The well-defined eddies present during summer (Figure 4c) enable a southward transport of nutrient-rich waters from the Iranian coast, while the relatively low wind speeds in the later summer and early autumn (Aboobacker et al., 2021a) cause their settling in the southern Gulf. Within the circumference of eddies, well-marked lower concentrations are evident during summer. The improved mixing conditions and a decline in SST facilitate nutrient resuspension in the offshore regions of the Gulf during autumn, as exhibited by a relatively higher Chl *a* compared to the summer.

Distinct spatial variability has been observed in the monthly mean Chl *a* concentrations (Figure 5). The Strait of Hormuz and the southern Iranian coast experience high Chl *a* during January and February, while the lowest is in June–August. This depicts the variations in the richness of nutrients in the inflow waters from the Sea of Oman and the role of shamal winds in controlling the circulations in the Gulf (Mussa et al., 2024). The observed seasonality along the Iranian coast, especially the region under the influence of IOSW (Nezlin et al., 2010), is similar to the typical tropical/subtropical ocean pattern, while the remaining Gulf coast has no such resemblances. Most of the Gulf basin experiences the lowest Chl *a* (< 1 mg/m^3) during April and May as the nutrient supply is very limited. The percentages of areas with concentration less than 1 mg/m^3 are 77% (April), 72% (May), 71% (June), 68% (March), 61% (July), and 56% (August). On the other hand, the southern and western shelves of the Gulf have the highest Chl *a* during August-October. These months mark the lowest mean wind speeds in the Gulf (Aboobacker et al., 2021a), while the inflow of IOSW, the eddies, and the ACC are stronger (Mussa et al., 2024). This helps to maintain a nutrient-rich surface layer along these shelves. A widespread Chl *a* distribution is notable during November, with the concentration exceeding 1 mg/m^3 accounting for 75% of the Gulf. Circulations in the Gulf are generally weaker during this month (Mussa et al., 2024). Whereas the hydrographic conditions and nutrient availability are

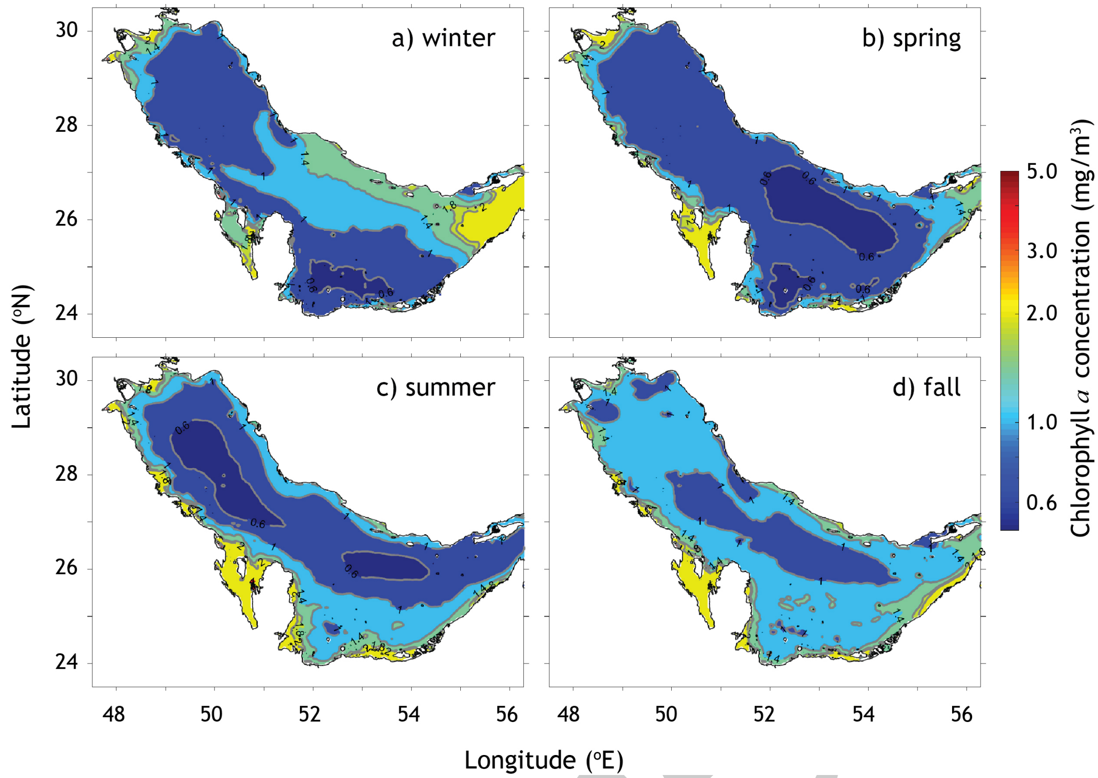

Figure 3. Mean Chl *a* during a) winter, b) spring, c) summer, and d) autumn for the period 1998–2022. Seasons are considered as DJFM, AM, JJAS, and ON, respectively.

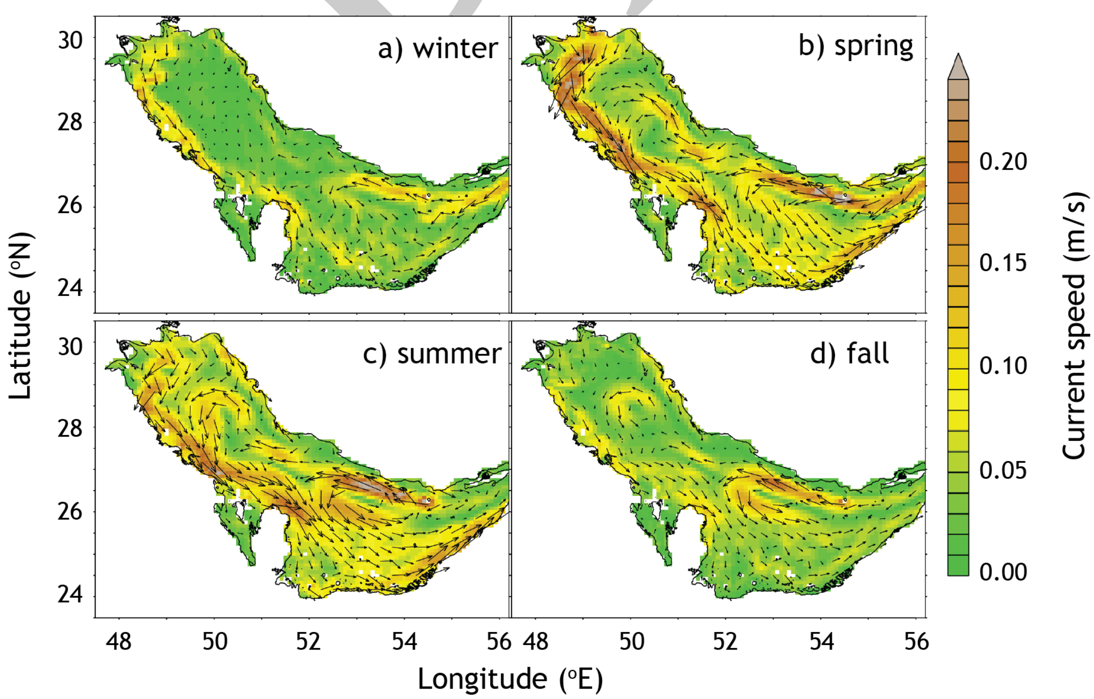

Figure 4. Surface mean current vectors and magnitudes during winter, spring, summer, and autumn for the period 1998–2022.

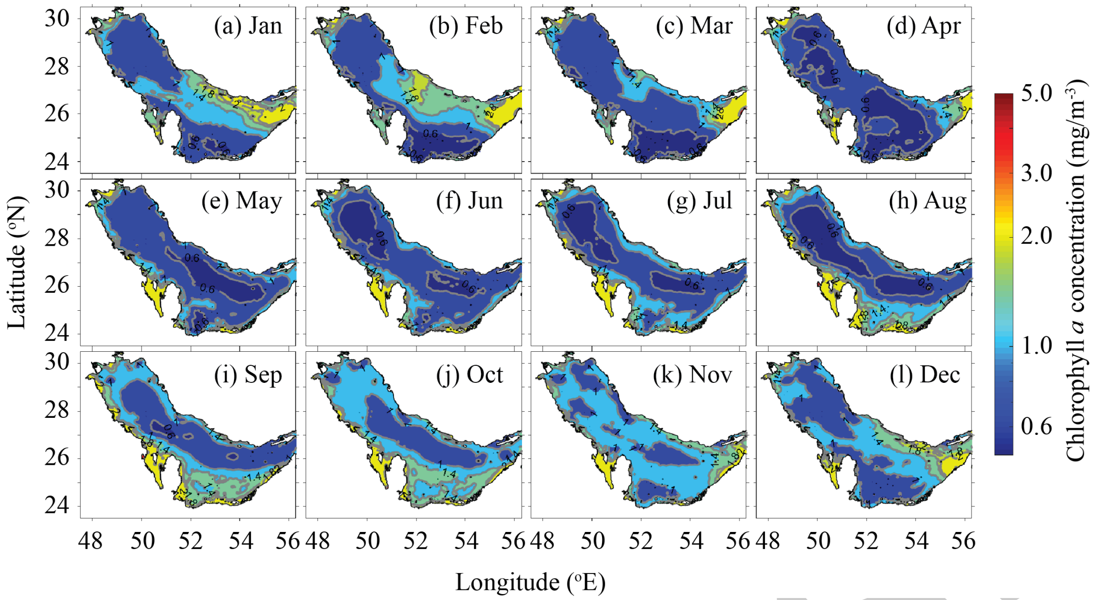

Figure 5. Monthly mean Chl *a* for the period 1998–2022.

in favor of this increased spatial distribution.

The monthly variability of Chl *a* concentrations at P1 to P5 is shown in Figure 6. At P1, the monthly mean Chl *a* is between 1.26 and 1.59 mg/m^3, where the seasonal variations are minimal. This suggests that the north station is a region of high primary productivity, due to consistent nutrient availability and favorable environmental conditions. This is because the river discharge is the main contributor of nutrients to this region, and the limited seasonal variability can be attributed to the difference in the river discharge. Moreover, the impact of overall Gulf circulation is weaker in this region. Being situated along the southern shelf of the Gulf basin, the monthly mean Chl *a* concentrations at P2 and P3 follow similar patterns, while the highest concentration occurs at P2. The range of mean concentrations at P2 and P3 is 0.98–2.14 and 0.63–1.82 mg/m^3, respectively. There exists strong seasonal variability in Chl *a* concentrations at these locations. The peak Chl *a* at P2 and P3 occurred during August and September, respectively. The lag of one month on the peak concentration is induced by the dynamics of the Gulf that alter the magnitudes of the flow. Mussa et al. (2024) identified a relatively higher mean current speed on the northern coast of Qatar during August compared to September, while the opposite is true along the southeastern coast of Qatar. The lowest Chl *a* at P2 and P3 occurred during February. This coincides with the highest shamal wind occurrence in the Gulf (Aboobacker et al., 2021a,b). The well mixing induced by shamal winds weakens the surface dominance of Chl *a* as the nutrients are re-distributed to the entire water column.

The mean Chl *a* at P4 and P5 are nearly the same except during December and January. Both locations are situated along the Iranian coast, where the influence of ICC is higher compared to the other areas of the Gulf. The ranges of mean concentrations at P4 and P5 are 0.75–1.74 and 0.77–1.94 mg/m^3, respectively. Seasonal variability is evident with lower concentrations during May and June, and higher concentrations during February and January, respectively at P4 and P5. This is directly linked to the seasonal variability of winds (Aboobacker et al., 2021a) and the circulation features (Mussa et al., 2024). An interesting feature observed between the southern shelves (P2 and P3) and the Iranian coast (P4 and P5) is the prevalence of Chl *a* concentration, which is inversely related, as illustrated in the monthly patterns. This pattern occurred due to the difference in the available Chl *a* in the Iranian coast by the action of winter shamal winds and to the southern shelves by the action of eddies and the prevalence of ACC. Overall, the Gulf's Chl *a* dynamics underscore a complex response to seasonal climatic patterns, water mixing characteristics, and nutrient dynamics.

4.4 Long-term linear trends in Chl *a*

It is evident from the previous analyses that the Gulf exhibits a complex and dynamic pattern of Chl *a*, with distinct regional variations and responses to external forcing factors. To assess the long-term temporal variability in Chl *a*, we further performed a linear trend analysis. Despite the lack of statistical significance, a positive trend is observed in the spatially averaged annual mean Chl *a* across the Gulf (Figure 7a). Nezlin et al. (2010) have shown that open waters in the Gulf were characterized by an overall positive trend, with short-term negative (1997–1999) and positive (2000–2002 and 2007–2008) anomalies. However, our results show that this increase is not uniform throughout the Gulf but has distinct regional variations influencing the overall picture. This is evident when analyzing the linear

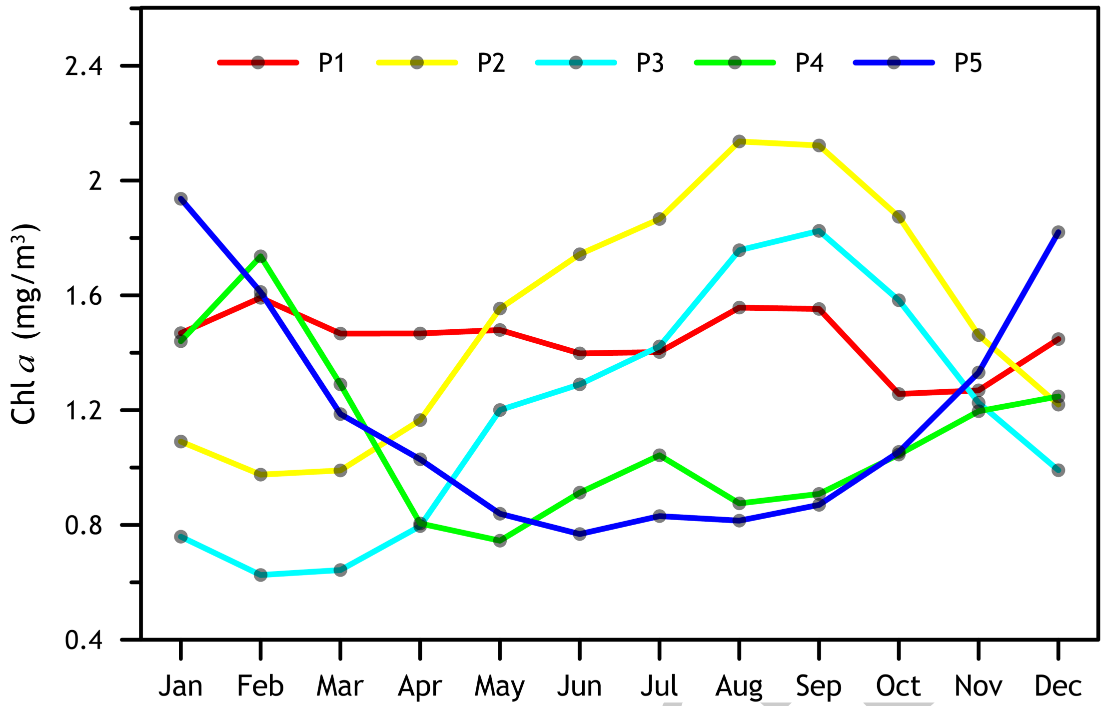

Figure 6. Monthly variability of Chl *a* at five select coastal stations.

trend in annual mean Chl *a* at P1 to P5 (Figure 7b–f). The Chl *a* concentrations at P1, P2, and P3 show an increasing trend during 1998–2022 with estimated rates of 0.0305, 0.0172, and 0.0242 mg/m^3/y, respectively. In contrast, the Chl *a* at P5 shows a weak decreasing trend, while that at P4 has no clear trends.

The observed increasing trend in Chl *a* concentrations across the Gulf, especially the northern (P1) and southern shelves (P2 and P3), is fascinating as far as the primary productivity is concerned. This highlights the complex

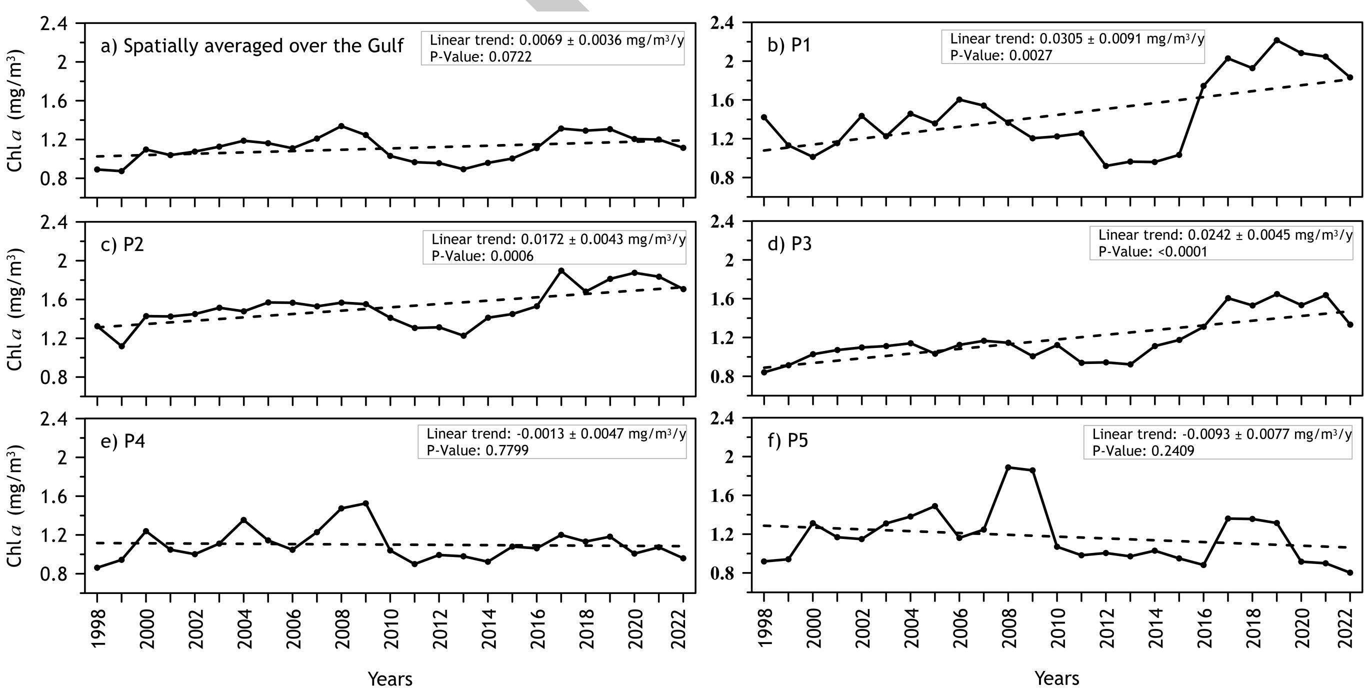

Figure 7. Interannual variability of mean Chl *a* at select stations.

Table 3. Results of multiple linear regression analysis. The stars represent the levels of significance for 3 of the most used levels. The correlation coefficient (r) with p-value < 0.001 is flagged with ***; with p-value < 0.01 is flagged with **; with p-value < 0.05 is flagged with *. Non-significant r values are not presented.

Model	P1		P2		P3		P4		P5	
	R^2	r	R^2	r	R^2	r	R^2	r	R^2	r
Chl *a* ∼ SST	0.00	–	0.69	0.83^{***}	0.60	0.77^{***}	0.16	0.4^{***}	0.17	0.41^{***}
Chl *a* ∼ WS	0.03	0.16^{**}	0.42	0.65^{***}	0.37	0.61^{***}	0.02	0.15^{**}	0.02	0.15^{**}
Chl *a* ∼ SLA	0.01	–	0.22	0.47^{***}	0.20	0.45^{***}	0.02	0.14^{*}	0.00	–
Chl *a* ∼ SST + SLA	0.01	–	0.75	0.86^{***}	0.66	0.81^{***}	0.16	0.40^{***}	0.17	0.41^{***}
Chl *a* ∼ SST + WS	0.03	0.16^{*}	0.71	0.84^{***}	0.61	0.78^{***}	0.19	0.44^{***}	0.19	0.44^{***}
Chl *a* ∼ WS + SLA	0.03	0.16^{*}	0.51	0.71^{***}	0.47	0.68^{***}	0.03	0.17^{*}	0.03	0.16^{*}
Chl *a* ∼ SST+ SLA + WS	0.03	0.18^{*}	0.76	0.87^{***}	0.67	0.82^{***}	0.19	0.44^{***}	0.19	0.44^{***}

interplay of regional factors and leads to potential implications for the ecosystem. The trend observed in the Gulf mirrors broader regional trends documented for the Sea of Oman and the Arabian Sea. Chinta et al. (2024) reported a decline in Chl *a* in the Sea of Oman at a rate of -0.088 mg/m^3/y, suggesting a broader regional shift in primary productivity. Roxy et al. (2016) further underscored this trend, predicting a potential decline in primary production for the Arabian Sea in the future. The observed consistent decline, particularly evident along the eastern coast of the Gulf bordered by Iran, suggests a shared influence from the Arabian Sea and the Sea of Oman. This could be due to a combination of factors such as climate change, altered upwelling patterns, or nutrient depletion within the Arabian Sea. The contrasting Chl *a* trends observed between the Iranian and Arabian coasts are likely driven by differences in nutrient availability. While the Iranian coast benefits from the nutrient influx from the Sea of Oman, the Arabian coast appears to rely more heavily on other nutrient sources. Al-Thani et al. (2023) reported the possibility of localized frontal upwelling based on their field measurements in the Qatar waters, which could contribute to nutrient enrichment in the southern Gulf. This suggests that factors such as riverine inputs (Moradi, 2020), atmospheric deposition (Asgari and Soleimany, 2023), localized upwelling (Al-Thani et al., 2023), and even precipitation (Nezlin et al., 2010) may play a more dominant role in sustaining primary productivity along the Arabian coast.

The increasing Chl *a* in the northern and southern Gulf could contribute to an increased risk of harmful algal blooms (HABs). The Gulf has experienced an increasing frequency and severity of HABs in recent decades (Al Shehhi et al., 2014; Al-Yamani et al., 2020). One such event was recorded in 2008–2009. These blooms can have detrimental effects, including marine life mortalities, as observed in Kuwait Bay (Al-Yamani et al., 2020), and impacts on human health through respiratory irritation (Al Shehhi et al., 2014; Tomlinson et al., 2009). The increased nutrient availability driving the Chl *a* increase may also exacerbate eutrophication, leading to oxygen depletion and further stress on marine organisms. The declining Chl *a* trend along the Iranian coast (P5) may indicate a reduction in primary productivity, potentially leading to food web shifts. A decrease in phytoplankton biomass could impact higher trophic levels, affecting fish populations and other marine organisms that rely on phytoplankton as a food source. This trend, coupled with the broader regional decline in Chl *a* observed in the Sea of Oman (Chinta et al., 2024) and the predicted decline in primary production for the Arabian Sea (Roxy et al., 2016), suggests a complex interplay of regional and local factors influencing primary productivity in the Gulf.

4.5 Relationship between Chl *a* and environmental factors

A multiple linear regression model has been applied to investigate the relationship between Chl *a* and possible environmental forcing factors such as SST, wind speed (WS), and sea level anomaly (SLA). Results show that the role of forcing factors has significant differences with different model combinations. The values of the coefficient of determination (R^2) and correlation coefficient (r) are given in Table 3. The individual correlation of SST and wind speed with Chl *a* is higher than that of SLA for all the selected stations. When the correlations with each of the independent variables are considered separately, the highest value was found for SST ($R^2 = 0.69$), followed by wind speed and SLA ($R^2 = 0.42$ and 0.22, respectively) at P2.

The data at P2 and P3 show significant correlation with higher values of r for all the combinations in the model; whereas the data at P1, P4, and P5 show relatively lower r values in most of the combinations of variables in the model, and they are not significant. The pairwise regression analysis indicates that the addition of SLA as an independent variable with SST increases the R^2 value by a modest 0.06 at both P2 and P3. That is, when SLA was added to the model along with SST, the increase in R^2 associated with the Chl *a* was only about 6%. Moreover, the addition of wind speed with SST in the model shows a similar correlation with Chl *a* concentration, without considerable changes in R^2 values. Unlike SST, SLA had a better association with wind speed in the pairwise regression, increasing

R^2 from 0.22 to 0.51, at location P2. Hence, wind speed contributed to a 29% variance in R^2 when combined with SLA in the model. Finally, with all variables taken together as independent variables, the explained variance (R^2) is 0.76 for all data, which is close to the result of the previous pairwise model with SST and SLA ($R^2 = 0.75$). Overall, the data show that SST has a stronger correlation with Chl *a* than wind speed and SLA, respectively. The stronger correlation we observed between SST and Chl *a* likely reflects the fundamental role of temperature in regulating phytoplankton growth and ecosystem dynamics. Temperature directly influences phytoplankton metabolic rates, water column stratification, nutrient availability, and species composition, all of which can impact Chl *a* concentrations (Doney et al., 2012).

4.6 Interannual variations and the influence of global climate oscillations

The interannual variations in basin-averaged annual mean Chl *a* reveal a clear pattern of peaks and troughs during the study period (Figure 7a). The years 2000, 2008, and 2017 are characterized by high Chl *a* levels, while a period of significantly low Chl *a* is observed from 2010 to 2014. This period of low Chl *a* is particularly pronounced at P1, P2, and P3 (Figure 7b,c,d). Post-2015, an increasing trend in annual mean Chl *a* is observed across most regions, indicating a rebound from the previous low period. This does not follow at P4 and P5. This regional anomaly could be attributed to various factors that need further investigation. The high Chl *a* observed in 2008 is most prominent at P5, indicating a localized influence on the regional distribution of Chl *a*. Conversely, the period of low Chl *a* from 2010 to 2014 is more intense at P1 and P2 compared to P3.

Studies have demonstrated that global climatic oscillations can significantly influence biological productivity in various oceanic regions (Barimalala et al., 2013; Cianca et al., 2012; Racault et al., 2017; Wiggert et al., 2009). The impact of these oscillations on Chl *a*, a key indicator of phytoplankton biomass and primary productivity, has been observed in different parts of the world's oceans. In the tropical Indian Ocean, Wiggert et al. (2009) showed that Chl *a* concentrations are impacted by Indian Ocean Dipole (IOD) events, highlighting the connection between large-scale climate patterns and regional biological productivity. Furthermore, Barimalala et al. (2013) found a notable impact of El Niño events on the Arabian Sea, reporting a 24% decrease in Chl *a* concentrations during winter. These findings highlight the importance of considering climate oscillations when studying the Chl *a* variations, especially at interannual time scales.

The basin-averaged annual mean Chl *a* overlaid with Oceanic Niño Index (ONI), Dipole Mode Index (DMI), and North Atlantic Oscillation (NAO) index is shown in Figure 8. The relationship between annual mean Chl *a* variability and climate indices is not linear. This is likely due to the co-existence of multiple climate phenomena and regional factors. ENSO, IOD, and NAO can exert a broad influence on global atmospheric circulation patterns, which in turn impact a variety of oceanographic processes, including wind patterns, SST, upwelling, and nutrient transport (Abish et al., 2018; Grunseich et al., 2011; Seelanki et al., 2022). To further investigate these associations in the Gulf, we performed a composite analysis of annual mean Chl *a* with respect to each climate index (Table 4). Composite analysis helps to isolate the signal of a specific climate event or phenomenon from the inherent variability of the climate system. By averaging data across multiple occurrences of the event, the signal is amplified while the random noise is suppressed. The years selected for the composite are (1) El Niño: 1998, 2003, 2007, 2010, and 2016; (2) La Niña: 1999, 2000, 2008, 2011, 2012, 2021, and 2022; (3) Positive IOD: 2006, 2012, 2015, and 2019; (4) Negative IOD: 1998, 2010, 2014, 2016, and 2021; (5) positive NAO: 2007, 2015, and 2020; and (6) negative NAO: 2010, and 2021.

The composite analysis of Chl *a*, wind speed, SST, and sea level anomaly (SLA) reveals the role of physical mechanisms that underpin the observed variability in Chl *a* concentrations during different phases of ENSO, IOD, and NAO (Table 4). During La Niña events, elevated Chl *a* levels across most stations (except P1) coincide with increased wind speed and SLA, while they are aligned with the cooler SST along the Iranian coast. La Niña reduces the inflow from the Arabian Sea to the Gulf, as large-scale circulations weaken (Jensen, 2007). The relatively warm water inflow from the Arabian Sea to the Gulf during winter is more prominent along the Iranian coast, while its reduction enhances the sea surface cooling by the effect of strong winter shamal winds. On the other hand, higher wind speeds and increased SLA enhance upwelling and vertical mixing in the Gulf, which increases the nutrient availability in the surface layer that is conducive to phytoplankton growth. This is consistent with the broader observations in the Indian Ocean that the interplay between cooler SSTs and stronger winds during La Niña years promotes favorable conditions for Chl *a* enhancement (Barimalala et al., 2013). This is also aligned closely with the results obtained in the Red Sea (Raitsos et al., 2015). Although the northern head of the Gulf (P1) responds quite differently, the basin-averaged values support the above observations. In general, ENSO can influence winter convective mixing and mixed-layer depth, thereby influencing the biological response of the Gulf significantly.

The composite analysis with IOD events reveals that the positive phases are aligned with an increase in Chl *a* and wind speed and with a decrease in SST and SLA (Table 4). The effect of IOD is quite complex in the Arabian Sea and adjacent areas, especially when they co-occur with ENSO. For instance, the co-occurrence of positive IOD and El Niño

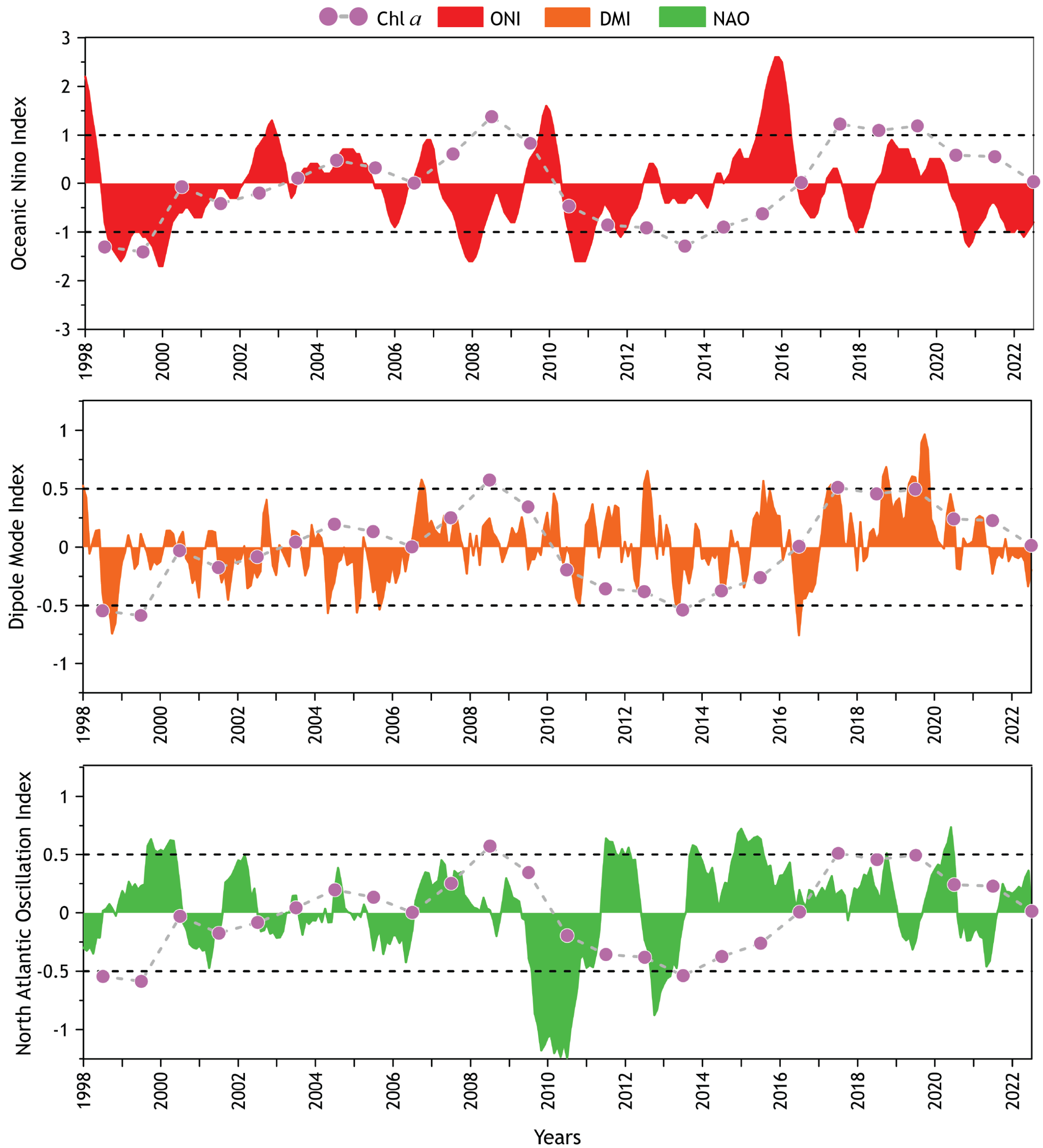

Figure 8. Climate indices of ENSO, IOD, and NAO overlaid with basin-averaged annual mean Chl *a*.

in the northern Arabian Sea reduces the Chl *a*, while an independent positive IOD increases the Chl *a* (Seelanki et al., 2022). However, irrespective of their co-occurrence, the results highlight an increase in Chl *a* (except at P1) during positive IODs, suggesting that positive IOD can favor increased primary production in the Gulf. At P1, higher Chl *a* occurred during negative IOD, which is supported by a lower SLA. This indicates that localised factors are more prevalent in the northern Gulf in determining the dominance of Chl *a* distribution than the direct impact of climatic oscillations such as IOD and ENSO.

The composite analysis of Chl *a* with NAO responds quite differently compared to that with ENSO and IOD (Table 4). Higher Chl *a* along the Arabian coast is observed during negative NAO, while that along the Iranian coast and most parts of the Gulf (basin-averaged) is observed during positive NAO. Whereas higher wind speeds have occurred during positive NAO, and lower SST and SLA have occurred during negative NAO, irrespective of the spatial distinction identified for the Chl *a* in the Gulf. Positive NAO enhances shamal winds that lead to relatively cooler SSTs in the Gulf during summer (Dasari et al., 2022; Lachkar et al., 2025).

Table 4. Composite of annual means of Chl *a*, SST, wind speed, and SLA during ENSO, IOD, and NAO events. Bold numbers indicate a higher value compared to their opposite phase.

	Station	El Niño	La Niña	pIOD	nIOD	pNAO	7nNAO
Chl *a* (mg/m^3)	P1	**1.43**	1.37	1.44	**1.48**	1.55	**1.64**
	P2	1.46	**1.47**	**1.54**	1.50	1.61	**1.62**
	P3	1.11	**1.13**	**1.22**	1.20	1.29	**1.38**
	P4	1.06	**1.08**	**1.08**	0.99	**1.11**	1.06
	P5	1.09	**1.12**	**1.11**	0.96	**1.04**	0.98
	Gulf-average	1.07	**1.08**	**1.09**	1.04	**1.14**	1.12
Wind speed (m/s)	P1	4.92	**5.05**	**5.02**	4.89	**4.98**	4.90
	P2	4.74	**4.93**	**4.79**	4.69	**4.82**	4.62
	P3	4.33	**4.46**	**4.41**	4.25	**4.44**	4.16
	P4	3.94	**4.08**	**3.98**	3.88	**3.98**	3.73
	P5	3.18	**3.22**	**3.21**	3.14	**3.18**	3.10
	Gulf- average	3.67	**3.75**	**3.73**	3.63	**3.74**	3.60
SST (°C)	P1	**24.97**	24.64	24.89	**25.14**	24.96	**25.39**
	P2	**26.68**	26.54	26.67	**26.92**	26.62	**27.19**
	P3	**27.87**	27.79	27.72	**28.07**	27.71	**28.39**
	P4	27.44	**27.47**	27.38	**27.67**	27.40	**28.08**
	P5	28.03	**28.10**	27.91	**28.20**	27.96	**28.54**
	Gulf- average	**26.99**	26.90	26.91	**27.19**	26.94	**27.50**
SLA (m)	P1	0.040	**0.047**	**0.063**	0.062	0.086	**0.099**
	P2	0.047	**0.056**	0.069	**0.080**	0.090	**0.107**
	P3	0.045	**0.064**	0.067	**0.073**	0.088	**0.102**
	P4	0.042	**0.054**	0.063	**0.065**	0.084	**0.097**
	P5	0.048	**0.060**	0.073	**0.074**	0.095	**0.103**
	Gulf- average	0.044	**0.056**	0.066	**0.069**	0.089	**0.101**

The winter shamal also shows a significant enhancement in the Gulf during positive NAO (Nelli et al., 2022). Amid increased wind speeds, cooler SST, and lower SLA, the reduction in Chl *a* during the positive NAO is a unique feature along the Iranian coast. This is primarily because of the changes in the circulation of the Arabian Sea and the Gulf. Strong winter shamal winds causes reduction in the inflow from the Arabian Sea and the general circulation in the Gulf (Asharaf et al., 2025; Mussa et al., 2023; Rafati and Rezazadeh, 2020). Such changes can directly impact the surface waters on the Iranian coast.

In general, climate oscillations can cause significant changes in physical-biological processes that arise from the changes in wind patterns, mixing, nutrient availability, and phytoplankton community composition. Given the intricate interplay between SST, wind speed, SLA, and biological productivity, and the spatial heterogeneity observed across the Gulf, further studies are essential to unravel the underlying mechanisms and improve predictive understanding of climate-driven marine ecosystem responses.

5. Conclusions

This study demonstrates the intricate relationship between climatic conditions, nutrient dynamics, and marine productivity in the Gulf based on merged satellite data obtained from CMEMS during 1998–2022. Results show that the northern head of the Gulf experiences a higher concentration of Chl *a* throughout the year due to the influence of the river Shatt-Al-Arab. Seasonal variations further illustrate the Gulf's dynamic ecosystem, with the winter showing enhanced Chl *a*, particularly along the Iranian coastal waters of the central and eastern Gulf, facilitated by nutrient-rich inflow from the Sea of Oman. On the other hand, the spring and summer are characterized by enhanced Chl *a* along the coasts of Kuwait, Saudi Arabia, Bahrain, Qatar, and the UAE, while a severe decline is identified along the Iranian coast. This is mainly due to the increased stratification, which inhibits nutrient mixing. Further, the less-nutrient inflow from the Sea of Oman during spring causes a depletion in the nutrient availability of the Gulf, which results in a lower Chl *a* concentration.

The trends in Chl *a* concentrations across the Gulf highlight the complex interplay of regional factors affecting primary productivity. A significant increasing trend is observed along the northern and southern shelves, while a notable decline is experienced along the Iranian coast, suggesting a shared influence from the adjacent Sea of Oman and the northern Arabian Sea, possibly due to altered upwelling or nutrient depletion. The observed contrasting trends along the Iranian coast likely result from differing nutrient sources. Multiple linear regression analysis shows the strongest correlation for SST than wind speed and SLA, highlighting its role in regulating phytoplankton growth. Composite analyses reveal that La Niña and positive IOD phases generally enhance Chl *a* across most of the Gulf, with a corresponding increase in wind speed and decrease in SST. Interestingly, the northern head of the Gulf exhibits a unique response; the Chl *a* levels increase during El Niño and negative IOD phases. Positive NAO enhances the Chl *a* in most parts of the Gulf, including the Iranian coast, while negative NAO enhances the Chl *a* along the Arabian coast, irrespective of the basin-scale consistency of wind speed, SST, and SLA with NAO. These provide a clear distinction between the two regions in the Gulf, supporting the role of localised effects on the Chl *a* distribution. Given the intricate interplay between SST, wind speed, SLA, and biological productivity, and the spatial heterogeneity observed across the Gulf, further studies are essential to unravel the underlying mechanisms and improve predictive understanding of climate-driven marine ecosystem responses.

Data availability

The GlobColour and sea level anomaly data used in the study were extracted from the CMEMS database, ERA5 winds from ECMWF, and sea surface temperature from AVHRR, which are freely available. The in situ data used for verification will be made available upon request.

Funding sources

This work was supported by the Qatar University (QU) Collaborative Grant (QUCG-ESC-22/23-591), which is covered under the UNESCO Chair in Marine Sciences at Qatar University.

Authors contribution

Cheriyeri Poyil Abdulla, Valliyil Mohammed Aboobacker, and Muhammad Shafeeque conceptualized and designed the study, prepared materials, collected data, and performed analyses. Cheriyeri Poyil Abdulla wrote the first draft of the manuscript. Valliyil Mohammed Aboobacker and Ponnumony Vethamony critically reviewed and edited the manuscript. All authors contributed to subsequent revisions, read, and approved the final version of the manuscript.

Acknowledgments

This work was funded by the Qatar University (QU) Collaborative Grant (QUCG-ESC-22/23-591). The work also falls under the scope of the UNESCO Chair in Marine Sciences at Qatar University. We express our gratitude to Prof. Hamad Al-Saad Al-Kuwari, Director of the Environmental Science Center (ESC) for his continuous encouragement and support. The satellite/reanalysis data used in this study were obtained from CMEMS, ECMWF, AVHRR, and AVISO.

Conflict of interest

None declared.

References

Abish, B., Cherchi, A., Ratna, S.B., 2018. *ENSO and the recent warming of the Indian Ocean*. Int. J. Climatol. 38 (1), 203–214. https://doi.org/10.1002/joc.5170

Aboobacker, V.M., Abdulla, C.P., Al-Ansari, E.M.A.S., Vethamony, P., 2024a. *Impacts of Shamal and Nashi winds on the hydrodynamics along the northeast coast of Qatar, central Arabian Gulf*. J. Coastal Res. 113, 609–613. https://doi.org/10.2112/JCR-SI113-120.1

Aboobacker, V.M., Hasna, V.M., Al-Ansari, E.M.A.S., Vethamony, P., 2024b. *Nearshore Hydrography along the Coast of Doha, Central Arabian Gulf*. J. Coastal Res. 113, 422–426. https://doi.org/10.2112/JCR-SI113-083.1

Aboobacker, V.M., Samiksha, S.V., Veerasingam, S., Al-Ansari, E.M.A.S., Vethamony, P., 2021a. *Role of shamal and easterly winds on the wave characteristics off Qatar, central Arabian Gulf*. Ocean Eng. 236, 109457. https://doi.org/10.1016/j.oceaneng.2021.109457

Aboobacker, V.M., Shanas, P.R., Veerasingam, S., Al-Ansari, E.M.A.S., Sadooni, F.N., Vethamony, P., 2021b. *Long-term assessment of onshore and offshore wind energy potentials of Qatar*. Energies 14 (4), 1178. https://doi.org/10.3390/en14041178

Ahmad, F., Sultan, S., 1991. *Annual mean surface heat fluxes in the Arabian Gulf and the net heat transport through the Strait of Hormuz*. Atmos. Ocean 29 (1), 54–61. https://doi.org/10.1080/07055900.1991.9649392

Al Senafi, F., 2022. *Atmosphere-ocean coupled variability in the Arabian/Persian Gulf*. Front. Marine Sci. 9, 809355. https://doi.org/10.3389/fmars.2022.809355

Al Shehhi, M.R., Gherboudj, I., Ghedira, H., 2014. *An overview of historical harmful algae blooms outbreaks in the Arabian Seas*. Mar. Pollut. Bull. 86 (1–2), 314–324. https://doi.org/10.1016/j.marpolbul.2014.06.048

Al-Ansari, E.M.A.S., Husrevoglu, Y.S., Yigiterhan, O., Youssef, N., Al-Maslamani, I.A., Abdel-Moati, M.A., Al-Mohamedi, A.J., Aboobacker, V.M., Vethamony, P., 2022. *Seasonal* *variability of hydrography off the east coast of Qatar, central Arabian Gulf*. Arab. J. Geosci. 15 (22), 1659. https://doi.org/10.1007/s12517-022-10927-4

Al-Mudaffar Fawzi, N., Mahdi, B.A., 2014. *Iraq's inland Water quality and its impact on the North-Western Arabian Gulf*. Marsh Bull. 9 (1).

Al-Naimi, N., Raitsos, D.E., Ben-Hamadou, R., Soliman, Y., 2017. *Evaluation of satellite retrievals of chlorophyll a in the Arabian Gulf*. Remote Sens-Basel. 9 (3), 301. https://doi.org/10.3390/rs9030301

Alosairi, Y., Alsulaiman, N., Petrov, P., Karam, Q., 2019. *Responses of salinity and chlorophyll a to extreme rainfall events in the northwest Arabian Gulf: Emphasis on Shatt Al-Arab*. Mar. Pollut. Bull. 149, 110564. https://doi.org/10.1016/j.marpolbul.2019.110564

Alosairi, Y., Imberger, J., Falconer, R.A., 2011. *Mixing and flushing in the Persian Gulf (Arabian Gulf)*. J. Geophys. Res.-Oceans 116 (C3). https://doi.org/10.1029/2010JC006769

Alosairi, Y., Pokavanich, T., 2017. *Residence and transport time scales associated with Shatt Al-Arab discharges under various hydrological conditions were estimated using a numerical model*. Mar. Pollut. Bull. 118 (1–2), 85–92. https://doi.org/10.1016/j.marpolbul.2017.02.039

Al-Said, T., Al-Ghunaim, A., Subba Rao, D., Al-Yamani, F., Al-Rifaie, K., Al-Baz, A., 2017. *Salinity-driven decadal changes in phytoplankton community in the NW Arabian Gulf of Kuwait*. Environ. Monit. Assess. 189, 1–17. https://doi.org/10.1007/s10661-017-5969-4

Al-Subhi, A.M., Abdulla, C.P., 2021. *Sea-level variability in the Arabian gulf in comparison with global oceans*. Remote Sens-Basel. 13 (22), 4524. https://doi.org/10.3390/rs13224524

Al-Thani, J.A., Soliman, Y., Al-Maslamani, I.A., Yigiterhan, O., Al-Ansari, E.M.A.S., 2023. *Physical drivers of chlorophyll and nutrients variability in the Southern-Central Arabian Gulf*. Estuar. Coast. Shelf Sci. 283, 108260. https://doi.org/10.1016/j.ecss.2023.108260

Al-Yamani, F.Y., Polikarpov, I., Saburova, M., 2020. *Marine life mortalities and harmful algal blooms in the Northern Arabian Gulf*. Aquat. Ecosyst. Health 23 (2), 196–209. https://doi.org/10.1080/14634988.2020.1798157

Amorim, F.L.L., Balkoni, A., Sidorenko, V, Wiltshire, K.H., 2024. *Analyses of sea surface chlorophyll a trends and variability from 1998 to 2020 in the German Bight (North Sea)*. Ocean Sci. 20 (5), 1247–1265. https://doi.org/10.5194/os-20-1247-2024

Anjaneyan, P., Kuttippurath, J., Kumar, P.H., Ali, S., Raman, M., 2023. *Spatio-temporal changes of winter and spring phytoplankton blooms in the Arabian Sea during the period 1997–2020*. J. Environ. Manage. 332, 117435. https://doi.org/10.1016/j.jenvman.2023.117435

Asharaf, M., Aboobacker, V.M., Abdulla, C.P., Joydas, T.V., Manikandan, K.P., Rafeeq, M., Al-Suwailem, A., Vethamony, P., 2025. *Perspectives of seasonal hydrography and water masses in Saudi waters of the Arabian Gulf*. Oceanologia 67 (4), 67407. https://doi.org/10.5697/KPCV6249

Asgari, H.M., Soleimany, A., 2023. *Long-term study of desert dust deposition effects on phytoplankton biomass in the Persian Gulf using Google Earth Engine*. Mar. Pollut. Bull. 195, 115564. https://doi.org/10.1016/j.marpolbul.2023.115564

Barimalala, R., Bracco, A., Kucharski, F., McCreary, J.P., Crise, A., 2013. *Arabian Sea ecosystem responses to the South Tropical Atlantic teleconnection*. J. Mar. Syst. 117, 14–30. https://doi.org/10.1016/j.jmarsys.2013.03.002

Behrenfeld, M.J., Falkowski, P.G., 1997. *Photosynthetic rates derived from satellite-based chlorophyll concentration*. Limnol. Oceanogr. 42 (1), 1–20. https://doi.org/10.4319/lo.1997.42.1.0001

Bordbar, M.H., Nasrolahi, A., Lorenz, M., Moghaddam, S., Burchard, H., 2024. *The Persian Gulf and Oman Sea: climate variability and trends inferred from satellite observations*. Estuar. Coast. Shelf S. 296, 108588. https://doi.org/10.1016/j.ecss.2023.108588

Chinta, V., Kalhoro, M.A., Liang, Z., Tahir, M., Song, G., Zhang, W., 2024. *Decadal climate variability of chlorophyll a in response to different oceanic factors in the Western Indian ocean: the Sea of Oman*. Clim. Dynam. 62 (9), 8675–8690. https://doi.org/10.1007/s00382-024-07354-4

Cianca, A., Godoy, J., Martin, J., Perez-Marrero, J., Rueda, M., Llinás, O., Neuer, S., 2012. *Interannual variability of chlorophyll and the influence of low-frequency climate modes in the North Atlantic subtropical gyre*. Global Biogeochem. Cy. 26 (2). https://doi.org/10.1029/2010GB004022

Currie, J.C., Lengaigne, M., Vialard, J., Kaplan, D.M., Aumont, O, Naqvi, S., Maury, O., 2013. *Indian Ocean dipole and El Nino/southern oscillation impacts on regional chlorophyll anomalies in the Indian Ocean*. Biogeosciences 10 (10), 6677–6698. https://doi.org/10.5194/bg-10-6677-2013

Dai, Y., Yang, S., Zhao, D., Hu, C., Xu, W., Anderson, D.M., Li, Y., Song, X.P., Boyce, D.G., Gibson, L., Zheng, C., 2023. *Coastal phytoplankton blooms expand and intensify in the 21st century*. Nature 615 (7951), 280–284. https://doi.org/10.1038/s41586-023-05760-y

Dasari, H.P., Ashok, K., Saharwardi, M.S., Luong, T.M., Masabathini, S., Vankayalapati, K., Gandham, H., Thiruridathil, R., Zamreeq, A., Ghulam, A., Abulnaja, Y., 2025. *Understanding and Predicting the November 24, 2022, Record-Breaking Jeddah Extreme Rainfall Event*. Meteorol. Applicat. 32 (5), p.e70100. https://doi.org/10.1002/met.70100

Devlin, M., Massoud, M., Hamid, S., Al-Zaidan, A., Al-Sarawi, H., Al-Enezi, M., Al-Ghofran, L., Smith, A.J., Barry, J., Stentiford, G.D., Morris, S., 2015. *Changes in the water quality conditions of Kuwait's marine waters: long-term impacts of nutrient enrichment*. Mar. Pollut. Bull. 100 (2), 607–620. https://doi.org/10.1016/j.marpolbul.2015.10.022

Devlin, M.J., Breckels, M., Graves, C.A., Barry, J., Capuzzo, E., Huerta, F.P., Al Ajmi, F., Al-Hussain, M.M., LeQuesne, W.J., Lyons, B.P., 2019. *Seasonal and temporal drivers influencing phytoplankton community in Kuwait marine waters: documenting a changing landscape in the Gulf*. Front. Marine Sci. 6, 141. https://doi.org/10.3389/fmars.2019.00141

Doney, S.C., Ruckelshaus, M., Duffy, J.E., Barry, J.P., Chan, F., English, C.A., Galindo, H.M., Grebmeier, J.M., Hollowed, A.B., Knowlton, N., Polovina, J., 2012. *Climate change impacts on marine ecosystems*. Annu. Rev. Mar. Sci. 4 (2012), 11–37. https://doi.org/10.1146/annurev-marine-041911-111611

El Hourany, R., Abboud-Abi Saab, M., Faour, G., Mejia, C., Crépon, M., Thiria, S., 2019. *Phytoplankton diversity in the Mediterranean Sea from satellite data using self-organizing maps*. J. Geophys. Res.-Oceans 124 (8), 5827–5843. https://doi.org/10.1029/2019JC015131

Elobaid, E.A., Al-Ansari, E.M.A.S., Yigiterhan, O., Aboobacker, V.M., Vethamony, P., 2022. *Spatial variability of summer hydrography in the central Arabian Gulf*. Oceanologia 64 (1), 75—87. https://doi.org/10.1016/j.oceano.2021.09.003

Ershadifar, H., Saleh, A., Kor, K., Ghazilou, A., Baskaleh, G., Hamzei, S., 2023. *Nutrients and chlorophyll a in the Gulf of Oman: high seasonal variability in nitrate distribution*. Deep-Sea Res. Pt. II 208, 105250. https://doi.org/10.1016/j.dsr2.2022.105250

Ford, D., Barciela, R., 2017. *Global marine biogeochemical reanalyses assimilating two different sets of merged ocean colour products*. Remote Sens. Environ. 203, 40–54. https://doi.org/10.1016/j.rse.2017.03.040

Ford, D.A., Edwards, K.P., Lea, D., Barciela, R.M., Martin, M.J., Demaria, J., 2012. *Assimilating GlobColour ocean colour data into a pre-operational physical-biogeochemical model*. Ocean Sci. 8 (5), 751–771. https://doi.org/10.5194/os-8-751-2012

Gao, K., Zhang, Y., Häder, D.P., 2018. *Individual and interactive effects of ocean acidification, global warming, and UV radiation on phytoplankton*. J. Appl. Phycol. 30, 743–759. https://doi.org/10.1007/s10811-017-1329-6

Garnesson, P., Mangin, A., Bretagnon, M., Jutard, Q., 2025. *Quality information document. Ocean Colour Production Centre*. https://documentation.marine.copernicus.eu/QUID/CMEMS-OC-QUID-009-101to104-111-113-116-118.pdf

Garnesson, P., Mangin, A., Fanton d'Andon, O., Demaria, J., Bretagnon, M., 2019. *The CMEMS GlobColour chlorophyll a product based on satellite observation: multi-sensor merging and flagging strategies*. Ocean Sci. 15 (3), 819–830. https://doi.org/10.5194/os-15-819-2019

Grunseich, G., Subrahmanyam, B., Murty, V.S.N., Giese, B.S., 2011. *Sea surface salinity variability during the Indian Ocean Dipole and ENSO events in the tropical Indian Ocean*. J. Geophys. Res.-Oceans 116 (C11). https://doi.org/10.1029/2011JC007456

Hankin, S., Harrison, D.E., Osborne, J., Davison, J., O'Brien, K., 1996. *A strategy and a tool, Ferret, for closely integrated visualization and analysis.* J. Visualizat. Computer Animat.7 (3), 149–157. https://doi.org/10.1002/(SICI)1099-1778(199607)7:3<149::AID-VIS148>3.0.CO;2-X

Heil, C.A., Glibert, P.M., Al-Sarawi, M.A., Faraj, M., Behbehani, M., Husain, M., 2001. *First record of a fish-killing Gymnodinium sp. bloom in Kuwait Bay, Arabian Sea: chronology and potential causes*. Mar. Ecol. Prog. Ser. 214, 15–23. https://doi.org/10.3354/meps

Hersbach, H., Bell, B., Berrisford, P., Hirahara, S., Horányi, A., Muñoz-Sabater, J., Nicolas, J., Peubey, C., Radu, R., Schepers, D., Simmons, A., 2020. *The ERA5 global reanalysis*. Q. J. Roy. Meteor. Soc. 146 (730), 1999–2049. https://doi.org/10.1002/qj.3803

Hussein, K.A., Al Abdouli, K., Ghebreyesus, D.T., Petchprayoon, P., Al Hosani, N., O. Sharif, H., 2021. *Spatiotemporal variability of chlorophyll a and sea surface temperature, and their relationship with bathymetry over the coasts of the UAE*. Remote Sens-Basel. 13 (13), 2447. https://doi.org/10.3390/rs13132447

Ismail, K.A., Al Shehhi, M.R., 2022. *Upwelling and nutrient dynamics in the Arabian Gulf and Sea of Oman*. Plos One 17 (10), e0276260. https://doi.org/10.1371/journal.pone.0276260

Jensen, T.G., 2007. *Wind-driven response of the northern Indian Ocean to climate extremes*. J. Clim.20 (13), 2978–2993. https://doi.org/10.1175/JCLI4150.1

Johns, W., Yao, F., Olson, D., Josey, S., Grist, J., Smeed, D., 2003. ObservationsofseasonalexchangethroughtheStraitsofHormuzandtheinferredheatandfreshwaterbudgetsofthePersianGulf. J. Geophys. Res.-Oceans 108 (C12). https://doi.org/10.1029/2003JC001881

Kämpf, J., Sadrinasab, M., 2006. *The circulation of the Persian Gulf: a numerical study*. Ocean Sci. 2 (1), 27–41. https://doi.org/10.5194/os-2-27-2006

Kendall, M., 1975. *Rank Correlation Methods*, 4th edn., Charles Griffin, London, 202 pp.

Keshavarzifard, M., Vazirzadeh, A., Sharifinia, M., 2021. *Occurrence and characterization of microplastics in white shrimp, Metapenaeus affinis, living in a habitat highly affected by anthropogenic pressures, northwest Persian Gulf*. Mar. Pollut. Bull. 169, 112581. https://doi.org/10.1016/j.marpolbul.2021.112581

Kim, H-J, Miller, A.J, McGowan, J., Carter, M.L., 2009. *Coastal phytoplankton blooms in the Southern California Bight*. Prog. Oceanogr. 82 (2), 137–147. https://doi.org/10.1016/j.pocean.2009.05.002

Lachkar, Z., Pauluis, O., Paparella, F., Khan, B., Burt, J. A., 2025. *Local and remote Climatic drivers of extreme summer temperatures in the Arabian Gulf*. EGUsphere, 2025, 1–30. https://doi.org/10.5194/egusphere-2025-2948

Mahmoodi, K., Ghassemi, H., Razminia, A., 2019. *Temporal and spatial characteristics of wave energy in the Persian Gulf based on the ERA5 reanalysis dataset*. Energy 187, 115991. https://doi.org/10.1016/j.energy.2019.115991

Maritorena, S., d'Andon, O.H.F., Mangin, A., Siegel, D.A., 2010. *Merged satellite ocean color data products using a bio-optical model: Characteristics, benefits, and issues*. Remote Sens. Environ. 114 (8), 1791–1804. https://doi.org/10.1016/j.rse.2010.04.002

Moradi, M., 2020. *Trend analysis and variations of sea surface temperature and chlorophyll a in the Persian Gulf*. Mar. Pollut. Bull. 156, 111267. https://doi.org/10.1016/j.marpolbul.2020.111267

Moradi, M., 2021. *Evaluation of merged multi-sensor ocean-color chlorophyll products in the Northern Persian Gulf*. Cont. Shelf Res. 221, 104415. https://doi.org/10.1016/j.csr.2021.104415

Moradi, M., Kabiri, K., 2015. *Spatio-temporal variability of SST and Chlorophyll a from MODIS data in the Persian Gulf*. Mar. Pollut. Bull. 98 (1–2), 14–25. https://doi.org/10.1016/j.marpolbul.2015.07.018

Moradi, M., Moradi, N., 2020. *Correlation between concentrations of chlorophyll a and satellite derived climatic factors in the Persian Gulf*. Mar. Pollut. Bull. 161, 111728. https://doi.org/10.1016/j.marpolbul.2020.111728

Mussa, A.A., Aboobacker, V.M., Abdulla, C.P., Hasna, V.M., Al-Ansari, E.M.A.S., Vethamony, P., 2024. *A climatological overview of surface currents in the Arabian Gulf with special reference to the Exclusive Economic Zone of Qatar*. Int. J. Climatol. 44(13), 4677–4693. https://doi.org/10.1002/joc.8603

Nelli, N., Francis, D., Fonseca, R., Bosc, E., Addad, Y., Temimi, M., Abida, R., Weston, M., Cherif, C., 2022. *Characterization of the atmospheric circulation near the Empty Quarter Desert during major weather events*. Front. Environ. Sci. 10, p. 972380. https://doi.org/10.3389/fenvs.2022.972380

Nezlin, N.P., Polikarpov, I.G., Al-Yamani, F.Y., Rao, D.S., Ignatov, A.M., 2010. *Satellite monitoring of climatic factors regulating phytoplankton variability in the Arabian (Persian) Gulf*. J. Mar. Syst. 82 (1–2), 47–60. https://doi.org/10.1016/j.jmarsys.2010.03.003

Niranjan Kumar, K., Ouarda, T., 2014. *Precipitation variability over the UAE and global SST teleconnections*. J. Geophys. Res.-Atmos. 119 (17), 10,313–10,322. https://doi.org/10.1002/2014JD021724

Pitarch, J., Volpe, G., Colella, S., Krasemann, H., Santoleri, R., 2016. *Remote sensing of chlorophyll in the Baltic Sea at basin scale from 1997 to 2012 using merged multi-sensor data*. Ocean Sci. 12 (2), 379–389. https://doi.org/10.5194/os-12-379-2016

Polikarpov, I., Saburova, M., Al-Yamani, F., 2016. *Diversity and distribution of winter phytoplankton in the Arabian Gulf and the Sea of Oman*. Cont. Shelf Res. 119, 85–99. https://doi.org/10.1016/j.csr.2016.03.009

Pous, S., Lazure, P., Carton, X., 2015. *A model of the general circulation in the Persian Gulf and in the Strait of Hormuz: Intraseasonal to interannual variability*. Cont. Shelf Res. 94, 55–70. https://doi.org/10.1016/j.csr.2014.12.008

Pramlall, S., Jackson, J. M., Konik, M., Costa, M., 2023. *Merged multi-sensor ocean colour chlorophyll product evaluation for the British Columbia coast*. Remote Sens-Basel. 15 (3), 687. https://doi.org/10.3390/rs15030687

Price, A.R.G., Sheppard, C.R.C., Roberts, C.M., 1993. *The Gulf: its biological setting*. Mar. Pollut. Bull. 27, 9–15. https://doi.org/10.1016/0025-326X(93)90004-4

Privett, D., 1959. *Monthly charts of evaporation from the N. Indian Ocean (including the Red Sea and the Persian Gulf)*. Q. J. Roy. Meteor. Soc. 85 (366), 424–428. https://doi.org/10.1002/qj.49708536614

R Core Team, 2023. *R: A Language and Environment for Statistical Computing*. R Foundation for Statistical Computing, Vienna, Austria. https://www.R-project.org/

Racault, M-F, Sathyendranath, S., Menon, N., Platt, T., 2017. *Phenological responses to ENSO in the global oceans*. Surv. Geophys. 38, 277–293. https://doi.org/10.1007/s10712-016-9391-1

Rafati, P. and Rezazadeh, M., 2020. *Correlation of NAO, IOD, and ENSO with the sea surface temperature changes in the Persian Gulf*. J. Earth Space Phys. 46 (2), 395–408. https://doi.org/10.22059/jesphys.2020.297756.1007198

Raitsos, D.E., Yi, X., Platt, T., Racault, M.F., Brewin, R.J., Pradhan, Y., Papadopoulos, V.P., Sathyendranath, S., Hoteit, I., 2015. *Monsoon oscillations regulate the fertility of the Red Sea*. Geophys. Res. Lett. 42 (3), 855–862. https://doi.org/10.1002/2014GL062882

Rajendran, S., Al-Naimi, N., Al Khayat, J.A., Sorino, C.F., Sadooni, F.N., Al Kuwari, H.A.,S., 2022. *Chlorophyll a concentrations in the Arabian Gulf waters of the arid region: A case study from the northern coast of Qatar*. Regional Stud. Marine Sci. 56, 102680. https://doi.org/10.1016/j.rsma.2022.102680

Rakib, F., Al-Ansari, E.M.A.S., Husrevoglu, Y.S., Yigiterhan, O., Al-Maslamani, I., Aboobacker, V.M., Vethamony, P., 2021. *Observed variability in physical and biogeochemical parameters in the central Arabian Gulf*. Oceanologia 63 (2), 227–237. https://doi.org/10.1016/j.oceano.2020.12.003

Rao, S., Al-Yamani, F., 1998. *Phytoplankton ecology in the waters between Shatt Al-Arab and Straits of Hormuz, Arabian Gulf: A review*. Plankton Biol. Ecol. 45 (2), 101–116.

Reynolds, R.M., 1993. *Physical oceanography of the Gulf, Strait of Hormuz, and the Gulf of Oman—Results from the Mt Mitchell expedition*. Mar. Pollut. Bull. 27, 35–59. https://doi.org/10.1016/0025-326X(93)90007-7

Ross, D.A., Uchupi, E., White, R.S., 1986. *The geology of the Persian Gulf-Gulf of Oman region: A synthesis*. Rev. Geophys. 24 (3), 537–556. https://doi.org/10.1029/RG024i003p00537

Roxy, M.K., Modi, A., Murtugudde, R., Valsala, V., Panickal, S., Prasanna Kumar, S., Ravichandran, M., Vichi, M., Lévy, M., 2016. *A reduction in marine primary productivity driven by rapid warming over the tropical Indian Ocean*. Geophys. Res. Lett. 43 (2), 826–833. https://doi.org/10.1002/2015GL066979

Saad, M.A., 1978. *Seasonal variations of some physicochemical conditions of Shatt al-Arab estuary, Iraq*. Estuar. Coast. Mar. Sci. 6 (5), 503–513. https://doi.org/10.1016/0302-3524(78)90027-0

Saha, K., Zhao, X., Zhang, H., Casey, K.S., Zhang, D., Baker-Yeboah, S., Kilpatrick, K.A., Evans, R.H., Ryan, T., Relph, J.M., 2018. *AVHRR Pathfinder version 5.3 level 3 collated (L3C) global 4km sea surface temperature for 1981 – Present*. NOAA Nat. Center. Environ. Informat., Asheville, NC, USA.

Schulzweida, U., 2023. *CDO User Guide (2.3.0)*. Zenodo. https://doi.org/10.5281/zenodo.10020800

Seelanki, V., Nigam, T., Pant, V., 2022. *Unravelling the roles of Indian Ocean Dipole and El-Niño on winter primary productivity over the Arabian Sea*. Deep-Sea Res. Pt. I 190, 103913. https://doi.org/10.1016/j.dsr.2022.103913

Sen, P.K., 1968. *Estimates of the regression coefficient based on Kendall's tau*. J. Am. Stat. Assoc. 63 (324), 1379–1389. https://doi.org/10.1080/01621459.1968.10480934

Shafeeque, M., Balchand, A.N., Shah, P., George, G., Smitha, B.R, Varghese, E., Joseph, A.K., Sathyendranath, S., Platt, T., 2021a. *Spatio-temporal variability of chlorophyll a in response to coastal upwelling and mesoscale eddies in the South Eastern Arabian Sea*. Int. J. Remote Sens. 42 (13), 4836–4863. https://doi.org/10.1080/01431161.2021.1899329

Shafeeque, M., George, G., Akash, S., Smitha, B.R., Shah, P., Balchand, A.N., 2021b. *Interannual variability of chlorophyll a and impact of extreme climatic events in the South Eastern Arabian Sea*. Regional Stud. Marine Sci. 48, 101986. https://doi.org/10.1016/j.rsma.2021.101986

Sheppard, C., Al-Husiani, M., Al-Jamali, F., Al-Yamani, F., Baldwin, R., Bishop, J., Benzoni, F., Dutrieux, E., Dulvy, N.K., Durvasula, S.R.V., Jones, D.A., 2010. *The Gulf: a young sea in decline*. Mar. Pollut. Bull. 60 (1), 13–38. https://doi.org/10.1016/j.marpolbul.2009.10.017

The MathWorks Inc., 2024. *MATLAB version: 24.2.0 (R2024b)*, The MathWorks Inc., Natick, Massachusetts, https://www.mathworks.com

Thoppil, P.G., Hogan, P.J., 2010. *Persian Gulf response to a wintertime shamal wind event*. Deep-Sea Res. Pt. I 57 (8), 946–955. https://doi.org/10.1016/j.dsr.2010.03.002

Tomlinson, M.C., Wynne, T.T., Stumpf, R.P., 2009. *An evaluation of remote sensing techniques for enhanced detection of the toxic dinoflagellate, Karenia brevis*. Remote Sens. Environ. 113 (3), 598–609. https://doi.org/10.1016/j.rse.2008.11.003

Vantrepotte, V., Mélin, F., 2009. *Temporal variability of 10-year global SeaWiFS time-series of phytoplankton chlorophyll a concentration*. ICES J. Mar. Sci. 66 (7), 1547–1556. https://doi.org/10.1093/icesjms/fsp107

Vaughan, G.O., Al-Mansoori, N., Burt, J.A., 2019. *The Arabian Gulf. World Seas: An Environmental Evaluation*. Elsevier, 1–23. https://doi.org/10.1016/B978-0-08-100853-9.00001-4

Veny, M., Aguiar-González, B., Marrero-Díaz, Á., Pereira-Vázquez, T., Rodríguez-Santana, Á., 2024. *Biophysical coupling of seasonal chlorophyll a bloom variations and phytoplankton assemblages across the Peninsula Front in the Bransfield Strait*. Ocean Sci. 20 (2), 389–415. https://doi.org/10.5194/os-20-389-2024

Volpe, G., Colella, S., Brando, V.E., Forneris, V., La Padula, F., Di Cicco, A., Sammartino, M., Bracaglia, M., Artuso, F., Santoleri, R., 2019. *Mediterranean Ocean Colour Level 3 operational multi-sensor processing*. Ocean Sci. 15 (1), 127–146. https://doi.org/10.5194/os-15-127-2019

Westberry, T.K., Silsbe, G.M., Behrenfeld, M.J., 2023. *Gross and net primary production in the global ocean: An ocean color remote sensing perspective*. Earth-Sci. Rev. 237, 104322. https://doi.org/10.1016/j.earscirev.2023.104322

Wiggert, J.D., Vialard, J., Behrenfeld, M.J., 2009. *Basin-wide modification of dynamical and biogeochemical processes* *by the positive phase of the Indian Ocean Dipole during the SeaWiFS era*. Indian Ocean biogeochemical processes and ecological variability, 185, 385–407. https://doi.org/10.1029/2008GM000776

Wright, J.L., 1974. *A hydrographic and acoustic survey of the Persian Gulf. Part I*. Naval Postgraduate School. https://doi.org/10.5962/bhl.title.60916

Xi, H., Losa, S.N., Mangin, A., Soppa, M.A., Garnesson, P., Demaria, J., Liu, Y., d'Andon, O.H., Bracher, A., 2020. *Global retrieval of phytoplankton functional types based on empirical orthogonal functions using CMEMS GlobColour merged products and further extension to OLCI data*. Remote Sens. Environ. 240, 111704. https://doi.org/10.1016/j.rse.2020.111704

Yu, S., Bai, Y., He, X., Gong, F., Li, T., 2023. *A new merged dataset of global ocean chlorophyll a concentration for better trend detection*. Front. Marine Sci. 10, 1051619. https://doi.org/10.3389/fmars.2023.1051619